12-3-2020

Novel High Isolation Antennas for Simultaneous Transmit and Receive (STAR) Applications

Alexander Hovsepian
ahovs001@fiu.edu

FLORIDA INTERNATIONAL UNIVERSITY

Miami, Florida

NOVEL HIGH ISOLATION ANTENNAS FOR SIMULTANEOUS TRANSMIT AND RECEIVE (STAR) APPLICATIONS

A dissertation submitted in partial fulfillment of

the requirements for the degree of

DOCTOR OF PHILOSOPHY

in

ELECTRICAL AND COMPUTER ENGINEERING

by

Alexander Hovsepian

2021

To: Dean John L. Volakis
College of Engineering and Computing

This dissertation, written by Alexander Hovsepian, and entitled Novel High Isolation Antennas for Simultaneous Transmit and Receie (STAR) Applications, having been approved in respect to style and intellectual content, is referred to you for judgment.

We have read this dissertation and recommend that it be approved.

_____
Shubhendu Bhardwaj

_____
Benjamin Boesl

_____
Stavros Georgakopoulos

_____
Elias A. Alwan, Co-Major Professor

_____
John L. Volakis, Co-Major Professor

Date of Defense: December 7, 2020

The dissertation of Alexander Hovsepian is approved.

_____
Dean John L. Volakis
College of Engineering and Computing

_____
Andrés G. Gil
Vice President for Research and Economic Development
and Dean of the University Graduate School

Florida International University, 2021

DEDICATION

Dedicated to my family.

ACKNOWLEDGMENTS

I would like to thank my committee members John Volakis, Elias Alwan, Shubhendu Bhardwaj, Stavros Georgakopoulos, and Benjamin Boesl for their constructive criticism and advice. I would like to give a special thank you to my co-advisor, Elias Alwan, who was a mentor from day one. Finally, I would like to express my gratitude to my advisor, John Volakis, for his transformative encouragement, guidance, and belief in me.

It was a pleasure working with Satheesh Bojja Venkatakrishnan on the topic of STAR. My fellow graduate students, Alexander Johnson, Jingni Zhong, Dieff Vital, Maxence Carvalho, and Matt Nichols, helped me immensely through our conversations on antennas. I would also like to acknowledge other researchers and graduate students who accompanied me on this journey: Abe, Dimitri, Carolina, Ray, Jorge, Rakibur, Rakibul, Asif, Kefayet, Alfredo, Ireen, and Mike. John Sahr's undergraduate antenna course in my final quarter steered me in this career direction. Additionally, I appreciate the numerous others who aided this endeavor.

To my parents, Rafi and Nancy, I am grateful for their gracious support and encouragement along these years.

ABSTRACT OF THE DISSERTATION

NOVEL HIGH ISOLATION ANTENNAS FOR SIMULTANEOUS TRANSMIT AND RECEIVE (STAR) APPLICATIONS

by

Alexander Hovsepian

Florida International University, 2021

Miami, Florida

Professor John L. Volakis, Co-Major Professor

Professor Elias A. Alwan, Co-Major Professor

Radio frequency (RF) spectrum congestion is a major challenge for the growing need of wireless bandwidth. Notably, in 2015, the Federal Communications Commission (FCC) auctioned just 65 MHz (a bandwidth smaller than that used for WiFi) for more than $40 billion, indicating the high value of the microwave spectrum. Current radios use one-half of their bandwidth resource for transmission, and the other half for reception. Therefore, by enabling radios to transmit and receive across their entire bandwidth allocation, spectral efficiency is doubled. Concurrently, data rates for wireless links also double. This technology leads to a new class of radios and RF frontends. Current full-duplex techniques resort to either time- or frequency-division duplexing (TDD and FDD respectively) to partition the transmit and receive functions across time and frequency, respectively, to avoid self-interference. But these approaches do not translate to spectral efficiency.

Simultaneous transmit and receive (STAR) radios must isolate the transmitter from the receiver to avoid self-interference (SI). This SI prevents reception and must therefore be cancelled. Self-interference may be cancelled with one or more stages

involving the antenna, RF or analog circuits, or digital filters. With this in mind, the antenna stage is the most critical to reduce the SI level and avoid circuit saturation and total system failure.

This dissertation presents techniques for achieving STAR radios. The initial sections of the dissertation provide the general approach of stage to stage cancellation to achieve as much as 100 dB isolation between the receiver and transmitter. The subsequent chapters focus on different antennas to achieve strong transmit/receive isolation. As much as 35 dB isolation is shown using a new spiral antenna array with operation across a 2:1 bandwidth. Also, a new antenna feed is presented showing 42 dB isolation across a 250 MHz bandwidth. Reflections in the presence of a dynamic environment are also considered.

TABLE OF CONTENTS

CHAPTER PAGE

LIST OF TABLES

TABLE PAGE

LIST OF FIGURES

FIGURE PAGE

ACCRONYMS AND ABBREVIATIONS

ADC	Analog to Digital Converter
AR	Axial Ratio
AUT	Antenna Under Test
BW	Bandwidth
Co-Pol	Co-Polarization
dB	Decibel
EM	Electromagnetic
F	Noise Factor
FCC	Federal Communications Commission
FDD	Frequency Division Duplexing
FSS	Frequency Selective Surface
GHz	Gigahertz
IL	Insertion Loss
ISM	Industrial, Scientific and Medical
LHCP	Left-Hand Circular Polarization
LNA	Low Noise Amplifier
LOS	Line of Sight
MHz	Megahertz
NF	Noise Figure
P2P	Point-to-Point
PA	Power Amplifier

PCB	Printed Circuit Board
RF	Radio Frequency
RHCP	Right-Hand Circular Polarization
Rx	Receive
SDR	Software Defined Radio
SI	Self-Interference
SMA	SubMiniature version A
SMP	SubMiniature Push-on
SMT	Surface Mount Technology
SNR	Signal to Noise Ratio
STAR	Simultaneous Transmit and Receive
TDD	Time Division Duplexing
TEM	Transverse Electromagnetic
Tx	Transmit
UHF	Ultra High Frequency
UWB	Ultra-Wideband
VHF	Very High Frequency
VNA	Vector Network Analyzer
VSWR	Voltage Standing Wave Ratio
X-Pol	Cross Polarization

CHAPTER 1: INTRODUCTION

1.1 Introduction

Radio frequency (RF) spectrum in the 1-6 GHz band is in short supply and has spurred interest in spectral efficiency. With limited bandwidth, which is proportional to data rate, the accrescent mobile traffic [1] market needs more efficient techniques to support the growing number of devices. Specifically, global mobile data rates continue to grow by about 30% each year (see below).

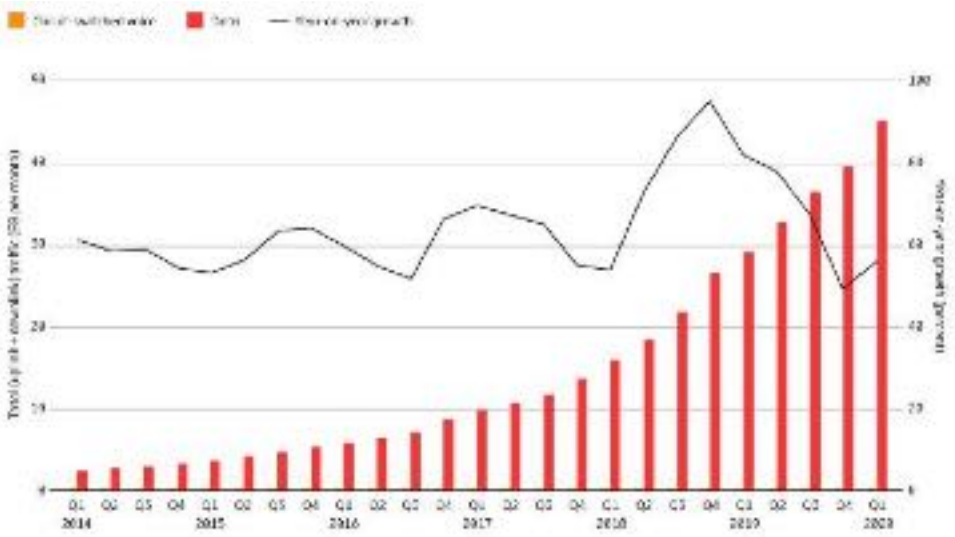

Figure 1 The mobile traffic data trend continues to grow [1].

Additionally, the strain on existing networks increases as the number of cellular IoT connections nearly doubled in the past two years at the time of this writing [2]. Despite the rollout of 5G, 4G will continue to be the most common IoT connection [2]. While new 5G bands are available, such as 28 GHz and 70 GHz, the 1-6 GHz band remains beneficial with its optimal transmission characteristics. Mobile providers and telecommunications companies are desperately attempting to reassign traditionally open spectrum allocations for exclusive licensing, such as the 3.3 GHz unlicensed amateur

bands [3] [4]. This indicates the continued value of the 1-6 GHz bands. Notably, RF spectrum market value has reached a premium, and in 2015, the Federal Communications Commission (FCC) auctioned a small 65 MHz bandwidth for $41 billion [5]. For comparison, this is smaller than 2.4 GHz WiFi's bandwidth. Clearly, achieving greater spectral efficiency has the potential to significantly reduce a licensee's spectrum costs. However, the amount of RF spectrum is fixed and new frequencies cannot be created due to physical limits. The spectrum chart below shows the dense frequency assignments from just 1 GHz of bandwidth [6].

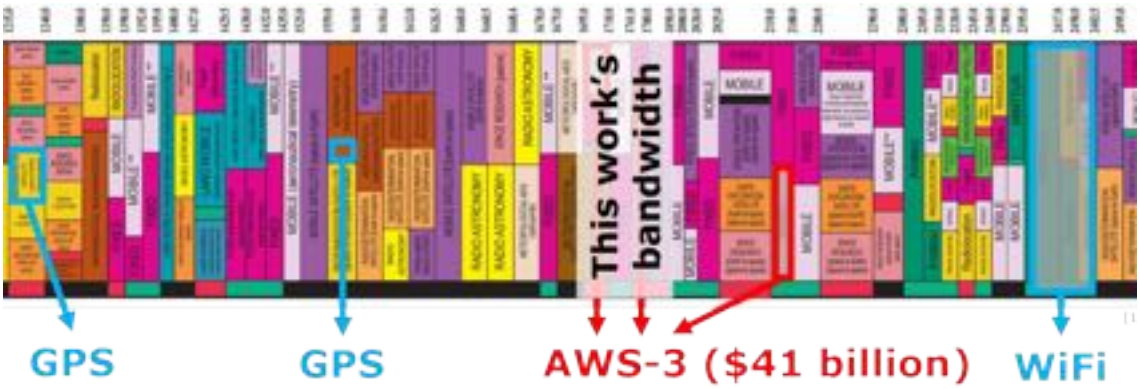

Figure 2 Congested radio frequency spectrum chart showing the many applications vying for access [6].

Objectives to increase spectral efficiency, such as higher order modulation techniques and channel encoding, have demonstrated success. However, these methods are capped by the system's power handling and dynamic range. The lower limit is restricted by the noise floor and the upper by FCC transmit power regulations for health safety. In this view, one such method to increase spectral efficiency is simultaneous transmit and receive (STAR). STAR enables concomitant reception with spectrum

assigned for transmission, promoting frequency reuse [7]. Alternatively, the required spectrum footprint can be reduced by up to 50%, reducing expensive licensing fees.

A key challenge with STAR is the transmitter's (Tx) self-interference (SI) that couples to the receiver (Rx). As expected, transmit/receive (Tx/Rx) coupling drastically lowers the receiver's dynamic range and can potentially desensitize it to any received signal. To avoid such leakage and therefore increase receiver sensitivity, methods such as time- and frequency-division duplexing (TDD/FDD) were adopted. In these cases, the Tx/Rx functions are partitioned in time and frequency respectively at the expense of spectral efficiency. Alternatively, to avoid saturation we may instead consider high isolation between the transmit and receive signals [7].

STAR systems may use one or more of the following methods to achieve transmit/receive (Tx/Rx) isolation: high isolation antennas, microwave or analog filters, digital filters, or absorbers/lossy materials. Additionally, STAR systems usually concatenate several of these to achieve over 100 dB isolation, which can be considered a minimum required system isolation level [8].

In the antenna domain, several techniques include orthogonal polarizations, bistatic configurations, circulators, physical symmetry with antipodal feeding, array beamforming, or mutual coupling resonators.

Further in the chain, microwave and digital filters may tap the transmit signal and then inject an inverted and scaled copy into the receiver, lowering the total SI. Due to the extreme level of required isolation, absorber materials may assist but cannot replace these stages. The focus of this work is on the antenna isolation stage as it is critical to ensure the receiver is not saturated by the large power coupled from the transmitter. Universally,

an antenna is the transducer between electrical signals in a circuit and radiating electromagnetic waves. All radios contain at least one.

This dissertation focuses on antennas and contributes two new designs. The first contribution is a new wideband spiral array for STAR with beam steering capability. The second is a novel Tx SI cancellation technique that incorporates feed tuning to enhance excitation symmetry, and therefore isolation.

1.2 Review of Key Antenna Properties

The antenna is a key component in every radio as it is the transducer between electric currents in a circuit and propagating electromagnetic (EM) waves. In transmission mode, the currents feeding the antenna radiate outward. During reception, incoming waves induce currents at the feed which are transferred to the backend circuitry.

The field of antennas began in the late 19th century, however the most significant improvements to bandwidth and adaptable antennas occurred in the 21st century. Heinrich Hertz is credited with developing the first antenna in an 1888 experiment and verifying important properties, such as the speed of radio waves [9]. Another important property is their reciprocal nature, implying its receive performance is identical to its transmit. This is convenient because one configuration may be simpler to realize and measure. For example, in antenna measurement chambers, called anechoic chambers, antennas under test (AUT) are generally placed in the receive configuration.

All antennas can be characterized by several properties. Their bandwidth is the range of frequencies where all the following characteristics reach acceptable values.

While there are no inherently correct or incorrect levels, industry and academia have generally adhered to standard conventions.

The input impedance is the ratio of electric to magnetic field strengths at the feed. However, this is not directly measurable, but it is easily inferred by comparing the input and reflected signals. This property is usually reported by the voltage standing wave ratio (VSWR) or return loss. The accepted maximum VSWR for narrowband antennas is 2, but relaxed to 3 in some cases, usually for ultra wideband (UWB) designs. Practically, this corresponds to a 90% and 75% transmission efficiency, respectively.

The radiation pattern refers to the 3-dimensional shape of the spatial distribution of power. Of the three categories, isotropic, omnidirectional, and directional, only the latter two are used. The isotropic pattern is a theoretical shape with equal power in all directions and is proven to not be possible to physically build. Omnidirectional patterns radiate equal power in only one plane and are advantageous for communication in all directions or an unknown one. Examples include AM or FM towers, aircraft voice communication, and vehicle FM antennas. Directional antennas have a single direction of peak radiation, such as a satellite dish antenna. As a key property, radiation pattern is important to characterize. This may be accomplished with several measurement types, each with its own merit. The antenna pattern measurement chambers with the smallest physical dimensions are near-field chambers. The far-field, which is seen by the receive antenna, can be calculated in post-processing through the more complicated near-field measurements. The advantages are lower size, cost, and maintenance compared to other methods. However, they are limited at lower frequencies due to antenna under test (AUT) to probe coupling effects. Another chamber is the compact range. Through the use of a

specially designed reflector, it is possible to create the plane wave a receive antenna would see in a reduced size, indoor facility. The reflector's 3-dimensional curvature is optimized so that there exists a zone where the incoming wave is phase coherent. This enables frequencies lower than the near-field chambers. The downside is for array measurements as the rotation of the center column must be factored into the post-processing to obtain accurate results. Finally, larger, outdoor chambers are suited for even lower frequency or larger prototype measurements.

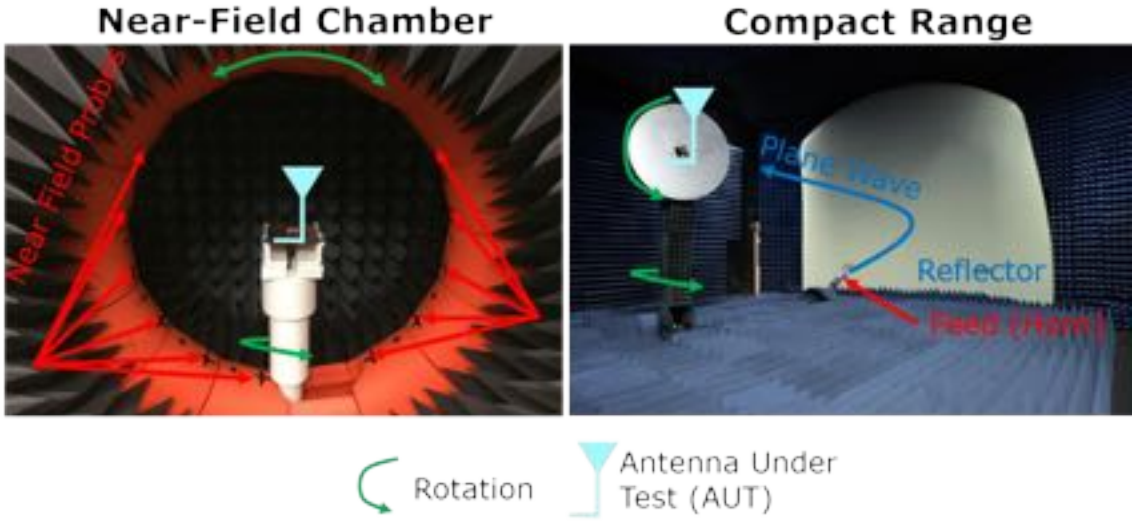

Figure 3 Antenna pattern measurements can be conducted in chambers of various sizes.

Table I Comparison of Compact Range and Near-Field Chamber Characteristics

Criteria	Near Field	Compact Range
Measurement Time	**Faster** ✓	Slower
Accuracy	Less	**Greater** ✓
Low Frequency	650 MHz	**500 MHz** ✓
Far Field	Calculated	**Measured** ✓

The directivity is the peak value of the normalized radiation pattern compared to an isotropic pattern. Gain is the directivity including losses.

Polarization refers to the direction of the electric field vector. Both a wave and antenna can have a polarization. An antenna's polarization is defined as the polarization of the radiating wave in transmit mode [10]. There are three categories: 1) linear, 2) elliptical (of which circular is a subset), and 3) unpolarized. Alignment for linear antennas is crucial as radios with misaligned antennas may not function.

The desired polarization is referred to as co-polarization (co-pol) while the unintended as cross-polarization (X-pol).

Polarization purity is the quantitative relation between the gain of the co- and X-pol radiation. In the linear case, polarization purity is reported as the difference in magnitude between the co- and X-pols. For elliptical, the axial ratio (AR) specifies the ratio between the major and minor axes in the ellipse that the electric field traces out in time. The axial ratio of a circularly polarized wave is 1 or 0 dB.

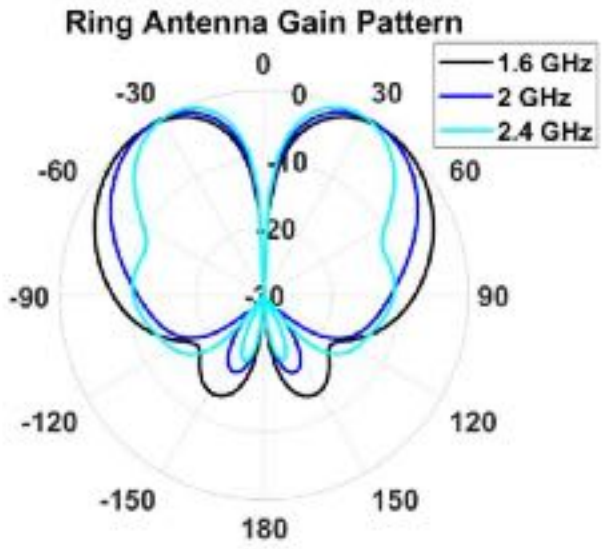

Figure 4 Vertical slice in an omnidirectional radiation pattern showing the nulls at boresight.

An important chart in ensuring the success of a wireless system is the link budget (see Table II). It determines the final receive power and noise floor by including estimates of environmental and antenna properties. A critical factor is the gain of the transmit and receive antennas. The gain is proportional to the receive power and affects the receive signal strength's upper limit. The lower limit is the noise floor, determined by the channel's bandwidth and physical temperature. The ratio of these two values is the signal to noise ratio (SNR) which determines the maximum data rate.

As can be seen from the example link budget, the transmit power is 105 dB greater than the receive power. As such, receive circuitry are designed for lower power input signal operation. However, all radios with transmit (Tx) and receive (Rx) functions exhibit leakage. This high power leakage can be on the order of 10-30 dB lower than the Tx power. Thus, the receiver sees interference from its own transmitter around 75-95 dB

greater than the intended signal. This power is too high and interferes with reliable reception.

To mitigate this Tx/Rx leakage, two methods were developed that avoid the transmitter and receiver from operating on the same frequency simultaneously. In time-division duplexing (TDD), both Tx and Rx use the full channel bandwidth at different intervals. A switch is placed at the antenna feed to select between Tx or Rx mode. The advantages are lower insertion loss (IL), greater average data rate, and the maximum bandwidth usage. The downside is lack of continuity in time. In frequency-division duplexing (FDD), Tx and Rx operate continuously across separate frequency bands. While avoiding down-time is beneficial, it comes at the cost of a frequency guard gap and additional insertional loss, which reduces SNR.

Table II An example link budget showing the factors that affect signal loss and final signal to noise ratio at the receiver.

Name	Symbol	Unit	Value
Tranmitter			
Transmit Power	Ptx	mW dB	20
Transmit Gain	Gtx	dB	7
Transmit Gain tol	Gtx,tol	dB	-3
Input Z mismatch loss		dB	-0.51
Channel			
Distance	R	km	20
Distance Attenuation (1/r^2)	PL	dB	-26.02
Electrical Size (fMHz)	f	GHz	3
Electrical Size Attenuation (fMHz)	f	dB	-69.54
Atmospheric Attenuation	La/km	dB/km	0.7
Total Medium Attenuation	La	dB	-14
Polarization Mismatch	Lp	dB	-1
Path Loss Tolerance		dB	-2
Receiver			
Receive Gain	Grx	dB	7
Receive Gain tol	Grx,tol	dB	-3
Input Z mismatch loss		dB	-0.51
Receive Power	Prx	mW dB	-85.58
Receive Noise Figure	NF	dB	4
Receive Noise Temperature	Trx	K	300
Receive Noise Bandwidth	Wrx	MHz	10
Noise Power	Pnoise	mW	4.14E-11
Noise Power	Pnoise	mW dB	-103.83
Receive Signal to Noise Ratio	SNR	dB	18.25
Min Latency	Tlat	ms	0.067

However, the STAR radio architecture must isolate the Tx and Rx chains by this leakage amount, which is on the order of 90-120 dB. STAR components generally add 10-50 dB isolation so multiple stages are usually concatenated to achieve the total required isolation. As the first component, the antenna provides a critical function of reducing the initial self-interference to a level that does not saturate the receiver circuitry. As such, it is critical to ensure high isolation at the antenna stage. This may be done using single- or multi-antenna configurations.

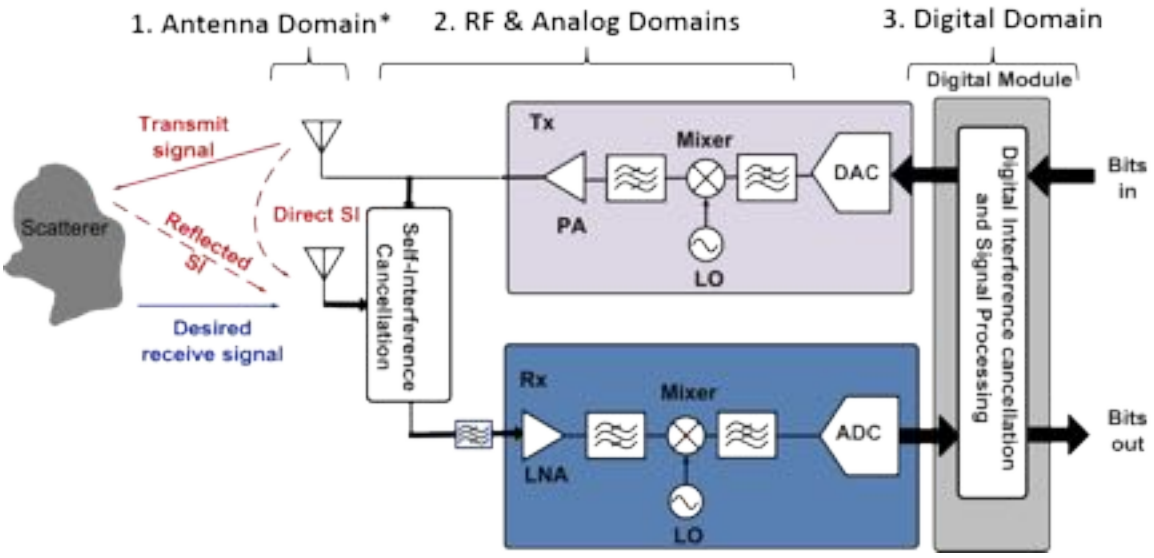

Figure 5 STAR radios can use a single- or multi-antenna configuration [11]. As such, standard microwave measurements with S-parameters can be used.

1.3 Simultaneous Transmit and Receive (STAR) Applications

Numerous applications could benefit from STAR, including telecommunications backhaul, satellite communications, cognitive radios, supervisory control and data acquisition (SCADA) networks, as well as point-to-point (P2P) microwave links. In the

future, as software defined radios (SDR) and low cost ultra wideband (UWB) antennas become prevalent, frequency agility will become as simple as a few lines of code. An economy of spectrum rental could immensely benefit from reduced bandwidth technology.

Figure 6 Photo of the antenna in a pump station in Miami, FL that could benefit from a STAR radio.

Notably, bi-static STAR was implemented in the 28 GHz 5G band, boasting data rates as high as 1.4 Gbps with an impressive 27 bps/Hz [12]. Here, separate antennas are used for transmission and reception. Transmit/receive isolation is based on very low mutual coupling between the two antennas. Commonly, microwave absorber is placed between the arrays in terrestrial systems. As land-based links can typically span several kilometers or more, spacing antennas has little impact on the path losses but significant improvement in isolation. A US-based startup implemented STAR in the UHF band with

analog and digital stages and achieved over 100 dB cancellation across a narrow 30 MHz bandwidth (240-270 MHz) [13]. Their plug and play product demonstrates the viability of practical STAR radios for rugged applications in the sub 1 GHz band.

1.4 Literature Review

Recent STAR realizations [7], [14]–[24] have successfully demonstrated 80-110 dB interference suppression. However, this was achieved over narrow bandwidths (i.e. 80 MHz) with fewer than three cancellation stages. To overcome this shortcoming, a novel wideband STAR radio with 4 stages of cancellation was proposed in [8], [25], & [26] by our group. Of importance is the radio's ability to cancel all linear, non-linear and transmit noise over the entire wide operational bandwidth.

Building on previous STAR radio realizations, we review different and improved STAR self-interference cancellation approaches at the antenna and RF stages.

A common radio configuration to minimize hardware is a single antenna architecture. In this case, full duplex is achieved by either time-division duplexing (TDD) or frequency-division duplexing (FDD). A feed network then divides the transmitter and receiver circuits [27]–[30] to isolate Tx and Rx. Such use of TDD or FDD wastes spectrum. Notably, TDD radios utilize circulators or isolators to achieve finite interference suppression between the Tx and Rx chains [31], [32]. Alternatively, multiple diplexers, which select for frequency, are required for multi-band or wideband systems. A major drawback is the significant interference from common modules (circulator/isolator/diplexer) connecting the Tx and Rx chains.

There are three paths for the high power Tx signals to couple into the Rx chain. These paths can be further divided into direct and in-direct interference components. Direct interference refers to signals that are coupled back to the receiver through cables or interconnects within the radio. The two direct interference components are: 1) coupling from the feed network component (circulator/isolator/diplexer) due to their finite isolation, referred to as direct interference from feed (DIF), and 2) reflection of Tx signals due to antenna mismatches, referred to as direct interference from the antenna or DIA [33]. Direct interference signal components can be determined analytically and removed. But the removal of in-direct interference from nearby reflectors, referred to as IIR, is more challenging. Unlike direct interference signals, cancellation circuits (in terms of filter order and components) are directly proportional to the desired cancellation at this stage. Higher order filters provide more cancellation. However, increased filter order affects the inter-modulation products (IP3) and noise figure among other parameters, thereby affecting the Rx chain performance [14], [34], [35]. Thus, it is desirable to achieve maximum cancellation at the antenna stage to relax the cancellation requirement at the RF level.

In this section, we discuss the main techniques to improve antenna isolation. These include techniques such as polarization diversity, physical separation, FSS/EBG structures for decoupling, enclosure within cavities or parasitic walls, and the inclusion of tunable elements to achieve symmetry in phase and magnitude.

Techniques have also been studied for increasing isolation between antenna array elements. Examples include digital beamforming for a linear array [36] to reduce Tx/Rx coupling across 125 MHz and a 2 by 2 patch antenna array [37] containing narrowband

filters operating across a 110 MHz bandwidth. However, previous implementations of inter-element coupling are narrowband with limited scanning efficiency. Isolation improvements were considered, but were limited to broadside arrays [38]. With this in mind, this section focuses on high isolation wide bandwidth STAR antenna arrays with wide angle scanning. It should be noted that the focus is to briefly summarize characterized high isolation antenna implementations.

1) Polarization Diversity

With polarization diversity, adjacent or collocated antenna elements have reduced coupling. Achieving this reduced coupling or isolation across a large bandwidth is even more challenging.

a) Linear polarization: Achieving improved isolation using orthogonal polarization greatly depends on the symmetry of the antennas and their feeds. To achieve this, even when scanning, the first step is to choose a UWB radiator, such as spiral or ring/monopole antennas.

b) Circular polarization: Circular polarization is preferred in certain cases as it leads to lower polarization mismatches in some applications. Indeed, slot spiral antennas [39] are known for their excellent circularly polarized (CP) radiation, low profile, and wideband performance.

However, to design a wideband beam steering spiral array, there are several key challenges to overcome. First, the spiral element must be miniaturized to achieve no grating lobes [40]. Often, the spiral diameter is larger to minimize reflections from the spiral arm terminations. To avoid this issue, a single matched resistor is introduced at the end of each slot arm to suppress reflections. Also, a balanced feed was introduced to

suppress interference between the Tx and Rx arms of this four-arm spiral. The 50 Ω to 120 Ω microstrip infinite balun was used in [39] to achieve balanced feeding. Notably, no separate balun was required, with significantly reduced size, weight, and power (SWaP). To ensure structural symmetry, dummy coaxial feeds were added as well. This led to higher isolation than previously recorded arrays of the same type. Full wave simulations of four-arm spiral arrays showed a high isolation of >40 dB across 1-5 GHz (5:1 bandwidth). This isolation was 11 dB lower at 30° scanning.

A 3×3 finite array simulation produced similar results. Also, measurements confirmed these simulations showing a 35 dB average Tx/Rx isolation. When scanning down to 30°, this isolation was reduced by a maximum of 9 dB. In terms of VSWR, no appreciable degradation was found across the entire bandwidth while scanning. Notably, a dual-pol linear antenna has orthogonal polarizations, however, in the case of the four-arm spiral both antennas transmit the same polarization, either RHCP or LHCP [38].

2) Exploiting Amplitude and Phase Balance

Another method to improve isolation in a multi-antenna radio is with a tunable balun that compensates for amplitude imbalances between the antenna feed branches. Above, we discussed use of symmetric structures and balanced feeding. However, the isolation level using this approach can be limited due to structural imperfections and manufacturing tolerances. This issue can be addressed with tunable baluns.

The concept of tunable baluns is depicted in a later chapter. In this case, a microstrip feed with a tapered ground plane is used to feed a circular loop. The feed is an exponential tapered microstrip balun which is 45mm long. To determine the approximate amplitude imbalance of the balun, two back-to-back baluns were fabricated. One balun

had inverted polarities connected (i.e., signal-ground of one balun connected to ground-signal of the other, respectively). The imbalance, or difference in S21s for the baluns, is estimated with measurements.

To compensate for the balun's current imbalance, an attenuator chip is inserted in each arm of the balun. The attenuator in the chip is controlled by a DC voltage bias. Specifically, while the antenna is in operation, the resistor value is altered via the bias voltage to achieve amplitude and phase control within the balun's arm. It should be noted that the insertion loss of the balun is about 1.4 dB. Measurements indicate that reliable control of the attenuation by step sizes of <0.1 dB is possible. This chip insert leads to 11 dB improvement in isolation. This resulted in an overall antenna isolation of 42 dB across 250 MHz. A major advantage of the attenuator chip is its tuning across a selected range of frequencies.

3) Other Decoupling Techniques

Physical separation is the simplest way to decouple a Tx and Rx antenna to reduce inter-element coupling. However, this approach adds to size and is not suited for arrays [19].

To avoid size and cost issues, inserts can be used to make the antenna to antenna separation electrically (not physically) larger. The simplest form of this approach is to use high permittivity and/or high permeability substrates. Another method is the introduction of periodic structures, either Frequency Selective surfaces (FSS), Electro-Band-Gap (EBG) structures, or high impedance surfaces that reject certain frequencies from propagating between antennas [41]–[43].

Using periodic structures, a wideband, bi-static, and dual-polarized simultaneous transmit and receive antenna subsystem was demonstrated with isolation >6 dB across the 6-19 GHz band. Specifically, a highly capacitive “bed of nails” was used to suppress TM polarized surface waves [44].

Another method of attenuating coupling signals between antennas is to use brute force attenuation or shielding of the adjacent elements. Techniques such as cavities, resistive walls, and lossy magnetics, can reduce coupling between adjacent elements at the cost of efficiency and space [45], [46].

Existing works showed wide bandwidths with Tx/Rx antenna isolation. The antenna in [47] measured 35 dB Tx/Rx isolation across 2-2.9 GHz, but required an external beamformer to improve to 50 dB. This method of wideband self-interference cancellation (SIC) used a circular array with progressive phases at each Tx element. In this case, the Tx feeds produced destructive interference at a central Rx element. Notably, wideband (0.6-3.3 GHz) isolation was demonstrated in [38] for a single element four-arm spiral. The paper in [38] was later expanded to a non-scanning seven element array [48] that showed 27 dB isolation across 0.65-2.7 GHz. Another variation of this approach used a two-layer circular ring [49]. In [50], a co-centric array of dipoles around a cone antenna achieved 37 dB of Tx/Rx isolation across 0.8-2.7 GHz. However, none of these designs considered scanning.

Several designs were capable of use in a beam steering system, but only for narrow bandwidths, as shown in Table I [37], [51]. For example, a linear array of dipoles in [51] relied on digital beamforming to reduce Tx/Rx coupling over a 100MHz bandwidth. Using Table I in [51], a Tx/Rx isolation of approximately 38 dB was inferred.

In [37], narrowband filters were used to cancel SI between adjacent elements across a 110 MHz bandwidth.

In 1991, a dual polarized microstrip antenna array [52] exploited the low cross polarization of the configuration to achieve high isolation. The authors of [53], [54], and [55] used rotational symmetry and a beamformer feed to cancel the transmit self-interference. Additionally, external circuits and microwave components were used to produce higher isolation. Similarly, [56] used patch antennas with feedforward isolation enhancements. The use of external circuits was an advantageous technique in [57] that combined aperture level and RF circuit level self-interference cancellation to achieve 20 dB, greater than simply antenna level isolation alone. Isolation with multi-stage components improved with the use of a multi-antenna STAR aperture with 3 quadrature hybrids. The authors showed 35 dB isolation across a 1.5 GHz bandwidth at 11-12.5 GHz using MMIC technology [58] [59]. This work was extended [60] by adding ferrite circulators to increase isolation. With optimization they achieved 60 dB Tx/Rx across 800 MHz at 10 GHz. Photonic systems offered isolation and bandwidth levels previously unmatched by radio frequency components. One such example was a decade bandwidth photonic STAR systems that relied on photonic circulators to achieve about 40 dB isolation in the X-band [61] [62]. This group further demonstrated a single-antenna architecture using the photonic circulators [63]. The next major improvement in STAR was proposed in [64], [65], and [66] by incorporating tunable resonators in patch arrays at around 3 GHz. Isolations of 30-40 dB were measured across narrow bandwidths of up to 110 MHz. For the first time, scanning was considered with a 2 by 2 patch array [37] with isolation measurements across various scan angles. However, these remained across

narrow bandwidths only. The use of self-cancelling transmit antennas was used in [67] where two transmits antennas were placed λ/2 offset relative to each other with a central receive feed.

Cancellation of transmit self-interference was demonstrated with measurements with two equi-spaced, antipodal monopoles with a central receive linear array of monopoles [68]. High isolation across wide bandwidths was demonstrated with a ring array prototype consisting of 8 co-centric monopoles with a central receive monopole [47]. Cancellation was achieved by a beamformer network feeding each transmit element with a progressive phase shift. Another prototype utilizing horn antennas with an identical cancellation technique was presented in [48]. Adaptive nulling in a dipole array achieved 30 dB cancellation across 12.5 MHz [69]. Further flexibility in designing multi-stage STAR systems was enhanced with a multi-tap delay filter for SI cancellation across a 100 MHz bandwidth in the 2.4 GHz band [70]. Notably, a company launched a STAR system with analog and digital SIC filters, however they did not publish their performance [71]. The feasibility of STAR at mm wave bands was discussed in [72]. Cancellation in scattering environment was considered in [73]. Simulations showing cancellation with filters placed between patch antennas extended this author's STAR work [37]. Photonics for intentional interference environments was discussed in [74]. Feed tuning in a 2-patch array cancelled reflected self-interference [75]. Simulations of a circular configuration showed wideband isolation with an antenna agnostic architecture [76]. Measured high isolation in a single-element 4-arm spiral was reported in [77]. An adaptive RF canceller was shown in [70]. Full STAR systems were shown in [78] and an outdoor test was demonstrated in [79]. Another paper [80] demonstrated 46 dB across a

2:1 bandwidth using a high precision manufactured reflector antenna. A design based on ferrite circulators achieved 40 dB isolation, but across a small 26 MHz bandwidth in the 900 MHz band [81].

Single-antenna architectures are less common than multi-antenna ones and achieve narrower bandwidths.

1.5 Wideband Scanning Array and Tunable Active Feed Contributions to STAR

This dissertation contributes two novel designs that advance the state-of-the-art. First, we introduce a STAR antenna array with wideband operation and beam steering capability. The array achieves a minimum of 35 dB measured isolation at broadside across a 2:1 bandwidth. Notably, when scanned to 30°, the total active isolation decreases by only 3 dB. This represents a 12× greater bandwidth over previous narrowband designs. Second, we demonstrate a novel tunable balun to reduce Tx/Rx coupling. A single chip is placed inside each arm of the balun to finely control its excitation amplitude. Balancing the currents enables precise destructive interference of the Tx self-interference at the Rx port. This mitigates the need for power hungry, bulky, and expensive backend circuity that accompany many STAR antennas.

CHAPTER 2: PASSIVE STAR ANTENNA – SINGLE-ELEMENT FOUR-ARM SPIRAL ANTENNA

2.1 Self-Isolating Antennas Based on Symmetry

A desirable quality of STAR antennas is their ability to isolate the Tx and Rx ports. A class of antennas that exhibit self-cancellation (see below) is the multi-antenna configuration that are balanced fed and have geometrical symmetry.

Figure 7 Symmetric, balanced fed antennas exhibit the self-cancellation property. Examples include cross dipoles, orthogonally fed patches, and four-arm spirals.

2.2 Design of a Miniaturized Single-Element Antenna with Self-Cancellation

Spirals are a class of frequency independent, traveling wave antenna. They operate across broad bandwidths with excellent circular polarization. Applications include ultra wideband communications and direction finding.

Spiral patterns have broadside lobes or nulls based on different feeds. Spirals operating in mode 1 (or odd modes) produce a broadside main lobe while mode 2 (or even modes) have boresight nulls. Mode 1 feeding is obtained with a balun (0° and 180° phases, specifically). Mode 2 patterns are created with in-phase feeds (0° and 0° phases).

The spiral arms' radius grows as their turn angle increases. The two most common arm growths are linear (called Archimedean) and exponential (called logarithmic) with respect to the turn angle. Spiral arms can be designed as metal or slots.

Spirals radiate efficiently if their aperture contains a ring with a circumference of one wavelength. An infinitely large spiral will have an infinite bandwidth. The ratio of the outermost to innermost circles indicates the bandwidth. The low frequency performance is determined by the outer edge while the high frequency is set by the inner portion.

A spiral can be viewed as a gradually growing loop. To intuitively understand mode 1 radiation, we can inspect one of these loops. Imagine a circle whose circumference is 1 λ. Pick a point on the outer edge as a reference. If we travel around the edge to the corresponding opposite point, we traveled $\lambda/2$. Half a wavelength corresponds to a 180° phase advance, which is the inverse of the first point. Radiation from these two points will cancel at broadside because the second point is 180° out of phase. However, in spirals these two points are on separate arms where the second arm is fed 180° out of phase. Thus, the second point undergoes two 180° shifts, or 360°, resulting in in-phase radiation at broadside.

The polarization is determined by the direction of curvature as the arms spread outward. Interestingly, opposite faces of the spiral radiate the opposite polarization sense due to the change in direction of the radiating wave.

Spirals arms are excited at their center. This can be through coaxial or printed circuit board feeds. Alternatively, an interesting and compact method for slot spirals integrates the balun on top of the spiral arms. The balun winds toward the outer edge where it can be fed with a 50 Ω connector or trace. This has also been adapted for use in four-arm spirals.

The four-arm spiral exhibits high isolation across all frequencies due to symmetry. We present a four-arm slot spiral antenna for use in STAR systems. Spiral antennas were selected for their excellent circularly polarized (CP) radiation and inherently wideband performance. In some applications, CP polarization is preferred to linear polarization due to unknown antenna orientations, such as in satellite or airborne communications. In each spiral, two arms are for transmit and the other two are for receive. Isolation is achieved through geometrical symmetry and the orthogonality of the Tx/Rx polarizations [38].

First, a miniature spiral element is required with a $\lambda_{HIGH}/2$ diameter to fit into a $\lambda_{HIGH}/2$ spaced array. Many spirals are 1 λ or even 2 λ in diameter. Clearly, such elements cannot be placed into a scanning array without unacceptable losses due to grating lobes. Second, we must maintain symmetry in the spiral arms, baluns, and feeds to ensure high Tx/Rx isolation.

Our miniaturized array element is based upon a previously developed single element square spiral [40]. Frequency independent isolation is achieved through

geometrical symmetry and the orthogonality of the Tx/Rx polarizations [38]. Each spiral element contains two arms for transmission and the other two for reception. Spiral antennas were selected for their excellent circularly polarized (CP) radiation and inherent wideband performance. In applications such as satellite or airborne communications, CP polarization is preferred as it minimizes polarization mismatch losses due to unknown antenna orientation or Faraday rotation [82].

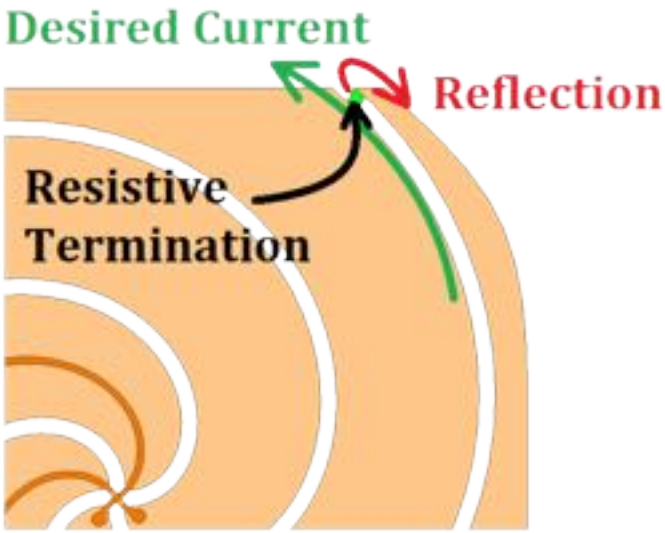

Figure 8 The resistive termination is optimized to reduce reflections at the end of the spiral arms.

2.3 Design and Fabrication

The antenna was designed to be fabricated on a 2-layer 10 mil thick substrate (RO4350B). The spiral arms are etched on the lower layer and the feed is placed on the upper layer. The array is backed by a ground plane at a distance of $\lambda_{HIGH}/3$. The slot arm growth rates are modified from an Archimedean spiral to improve the axial ratio at low frequencies. Each slot arm is terminated at the outer edge of the spiral by a surface mount

resistor placed across the end of the slot arm [40]. A microstrip infinite balun provides the balanced feeding for each Tx and Rx arm pair. Thus, no separate balun is needed behind the antenna. The microstrip feed was placed on the top layer and the spiral on the bottom layer. The microstrip is fed with coaxial cables through the ground plane. Ferrite beads are placed around the coaxial cables to reduce parasitic currents on the coaxial cables' outer shielding. The element's diameter was selected for increased bandwidth while maintaining the critical $\lambda_{HIGH}/2$ element spacing to avoid grating lobes. The highest frequency was set to 3.3 GHz. If the scan angle is limited to a specified value, the spiral elements could be further optimized for increased bandwidth and gain while avoiding grating lobes.

The spiral elements were designed for fabrication on a 2-layer PCB. The slot spiral arms were etched on the lower layer and the feed was placed on the upper layer. Each slot arm was terminated at the outer edge of the spiral by a surface mount resistor placed across the end of the slot arm [40]. The entire array was backed by a ground plane at a distance of approximately $\lambda_{LOW}/8$. A microstrip infinite balun provided the balanced feeding for each Tx and Rx arm pair. Thus, no separate balun was needed behind the antenna, reducing the antenna's size, weight, and power (SWaP), as well as cost. A 50 Ω coax cable through the ground plane fed the microstrip. Ferrite beads were placed around the coaxial cables to reduce parasitic currents on the outer shielding. Notably, each element was miniaturized [40] so that the element-to-element spacing was kept at $\lambda_{HIGH}/2$, ensuring no grating lobes (f_{HIGH} = 5 GHz). In terms of wavelengths, the diameter of each element was 0.2 λ_{LOW} = 0.5 λ_{HIGH}. To achieve the maximum gain and good matching with $\lambda_{HIGH}/2$ spaced elements, it was necessary to miniaturize the spiral

elements. An arm growth rate was of approximately 100 mil/radian. If the scan angle was limited to a specified value, the spiral elements could be further optimized for increased bandwidth and gain while avoiding grating lobes.

The four-arm relies on physical symmetry to produce high isolation. Thus, creating a symmetric spiral and balun are of great importance, especially at the upper frequencies of the antenna's bandwidth where features are electrically larger. A common balun for two-arm spirals is the infinite balun, which can be replicated for four-arm spirals. Each four-arm spiral will have two single-ended feeds. In the STAR four-arm spiral, one port is for Tx and the other port is for Rx. The resulting four-arm spiral infinite balun on a two-layer board is physically impossible due to the overlap at the center of the spiral. Previously, four-arm spirals that were fabricated on two-layer PCBs usually used an offset via to cross over. However, achieving high isolation at 5 GHz required a more symmetric balun. Placing a 0 Ω jumper across the top of the center of the spiral allows the feed to be placed on one layer on the PCB. Simulations showed the higher symmetry improves the minimum isolation by >7 dB. The authors also investigated three-layer designs where each balun's microstrip trace was placed on a separate layer, thus no crossover was required. However, this produced high isolation only at lower frequencies in the bandwidth. This cross-over configuration enables fabrication of higher frequency STAR spiral arrays with PCB techniques. The four-arm spiral model is shown below.

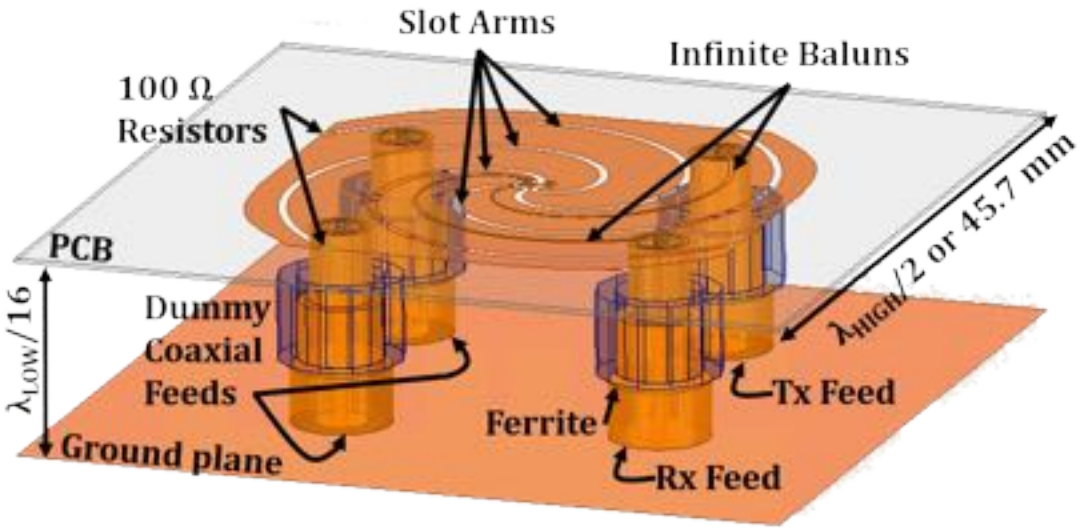

Figure 9 Design of the four-arm slot spiral showing the RF adapters and ferrite cores to suppress feed radiation.

The spiral antenna is on the printed circuit board (PCB) along with the balun. The balun was fed by a 50 Ω MMCX connector. The antenna PCB is attached to the ground plane by an MMCX adapter. Finally, the output is an MMCX to SMA adapter. To reduce currents on the MMCX adapter shields, ferrite cores were inserted. There are four feeds, one for Tx, one for Rx, and two dummies. These dummy feeds maintain the symmetry necessary for high isolation.

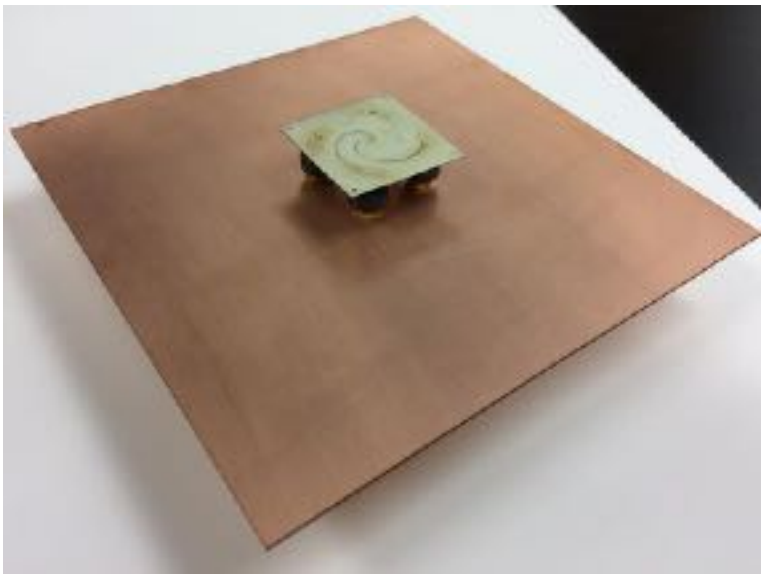

Figure 10 Photo of the fabricated single-element 4-arm spiral antenna with ferrite beads.

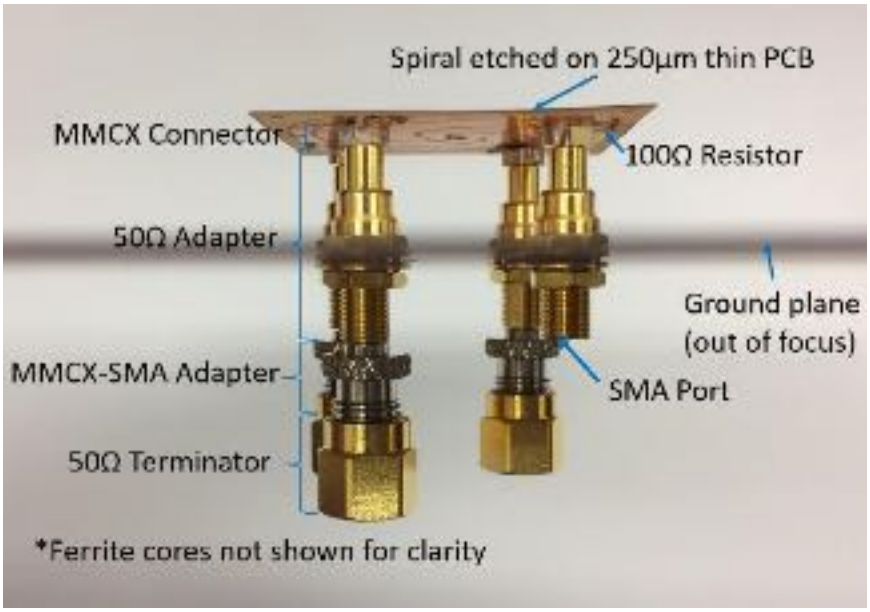

Figure 11 Photo detailing the assembly of the spiral element and ground plane using MMCX adapters that provide rigidity and modularity. This approach was replicated to form the array (the ferrite cores are removed for clarity).

2.4 Measurements and Conclusion

We measure the transmit/receive isolation with two-port S-parameter measurements, specifically S21. Measurements were taken with a vector network analyzer and showed excellent results for both VSWR and isolation across the entire bandwidth. To ensure no resonances existed causing high VSWRs, step sizes of 10 MHz were used.

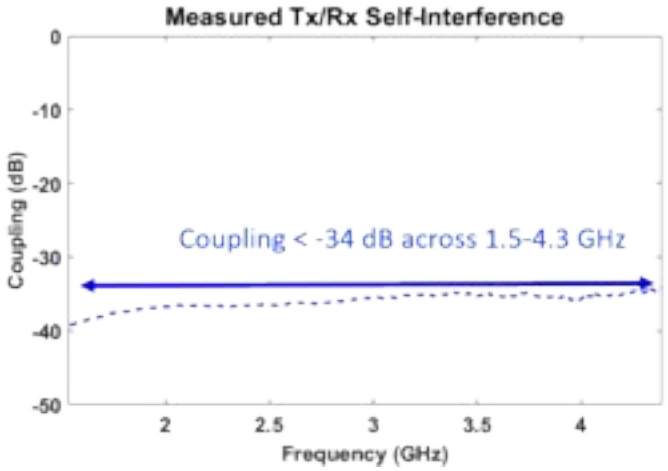

Figure 12 The four-arm spiral antenna showed high Tx/Rx isolation across its 1.5-4.3 GHz bandwidth.

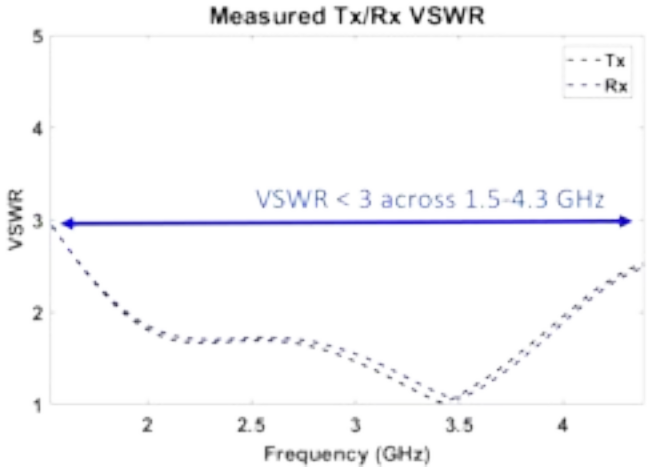

Figure 13 The VSWR < 3 for both Rx and Tx ports across its entire bandwidth.

CHAPTER 3: PASSIVE STAR ANTENNA – EXTENDING THE WIDEBAND SPIRAL TO ARRAYS

3.1 Obstacles to a Wideband Scanning Array for STAR

Simultaneous transmit and receive (STAR) is attractive because it doubles spectral efficiency and alleviates radio frequency (RF) spectrum congestion. As expected, a major challenge in STAR is the high power leakage from the transmitter to the receiver, which dramatically reduces a receiver's dynamic range and then leads to desensitization. Therefore, it is paramount to ensure high transmit/receive (Tx/Rx) isolation. Here, we present a wideband STAR antenna array operating across 1.6-3.28 GHz (1 octave bandwidth), with a large transmit to receive isolation of 35 dB across the entire bandwidth. This is the first wideband and low profile ($\lambda/16$ at the lowest frequency) STAR array retaining strong isolation when scanning down to 30° from broadside. The array elements are four-arm spirals where two arms are for transmit and the other two for receive. To ensure high Tx/Rx isolation, symmetry is maintained everywhere in the structure, spiral arms, baluns, and feeds. The element spacing is kept at $\lambda/2$ at the highest frequency to avoid grating lobes. A 5×5 array prototype was built and tested to validate the design. Measurements show excellent agreement with simulations.

Here, for the first time, we present a scanning array that achieves strong isolation across a wide bandwidth. The array consists of four-arm spiral elements. It achieves high Tx/Rx isolation when beam steering across a 2:1 instantaneous bandwidth (see Table III).

Table III Comparison of Scanning STAR Arrays

	Array	Frequency (GHz)	Bandwidth (%)	λ/2-spaced	Isolation (dB)	
					0°	30°
No Scan	[47]	2-2.9	37	Yes	35	--
	[38]	0.62-2.5	121	NA	39.6	--
	[48]	0.65-2.75	150	No	27	--
	[49]	0.9-2.5	94	No	28	--
	[50]	0.8-2.7	109	No	37	--
Scans	**[51]**	**2.4-2.5**	**4**	**Yes**	**38.3**	**NR**
	[37]	**3.45-3.5**	**2**	**Yes**	**40**	**25**
	This work	**1.6-3.28**	**68**	**Yes**	**35**	**32**

Notably, frequency independent isolation is achieved by ensuring geometrical symmetry, orthogonal polarizations [83], and balanced feeding in the four-arm spiral structure [38]. Concurrently, wideband scanning is achieved using a reduced size spiral [40] to ensure that center-to-center separation is at most $\lambda_{HIGH}/2$, where λ_{HIGH} is the wavelength at the highest frequency of operation. To our knowledge, this is the first wideband scanning array for STAR with potential applications in a phased array configuration. To achieve wideband scanning, we reduced the size of the four-arm spiral and incorporated a single load termination at the end of the spiral arms without compromising bandwidth. This work demonstrates, with new measurements, high isolation retention when scanning. Previous works did not [84] [85] [86] provide such

high isolation when scanning. Additionally, to enable high mutual isolation, the spiral antennas in this work were designed as single elements, not as a series of tightly coupled arms, as was the case in previous work.

To design and fabricate the proposed wideband beam steering array, we must address several challenges:

- Reduce the spiral's size [40] to achieve a maximum diameter of $\lambda_{HIGH}/2$ at the highest operating frequency;
- Suppress reflections from the spiral ends to enable low VSWR.
- Design the antenna element with high symmetry, when the balun and feed are taken into consideration.

Dummy feed components were added to ensure greater symmetry. Additionally, we used a microstrip infinite balun [39] for each pair of spiral arms to convert the 50Ω unbalanced coaxial input into a 130 Ω differential feed. Thus, no external balun was required, leading to reduced antenna size, weight, and power (SWaP).

To suppress grating lobes across the intended 1.6-3.28 GHz bandwidth, the spiral elements must be reduced in size. To do so, we used the miniaturization approach in [40]. Specifically, the design in [40] terminates the spiral arm ends with a resistor. The resistive termination in [40] replaced impedance tapers composed of multiple discrete resistors [87] with a single termination. As such, the length of each spiral arm was shortened, enabling array elements with diameters of $\lambda/2$ at 3.28 GHz.

The next section details the array design with full-wave simulations for infinite and finite arrays. Further, we discuss several design challenges for wideband scanning. Finally, we present measurements to assess the array's Tx/Rx isolation.

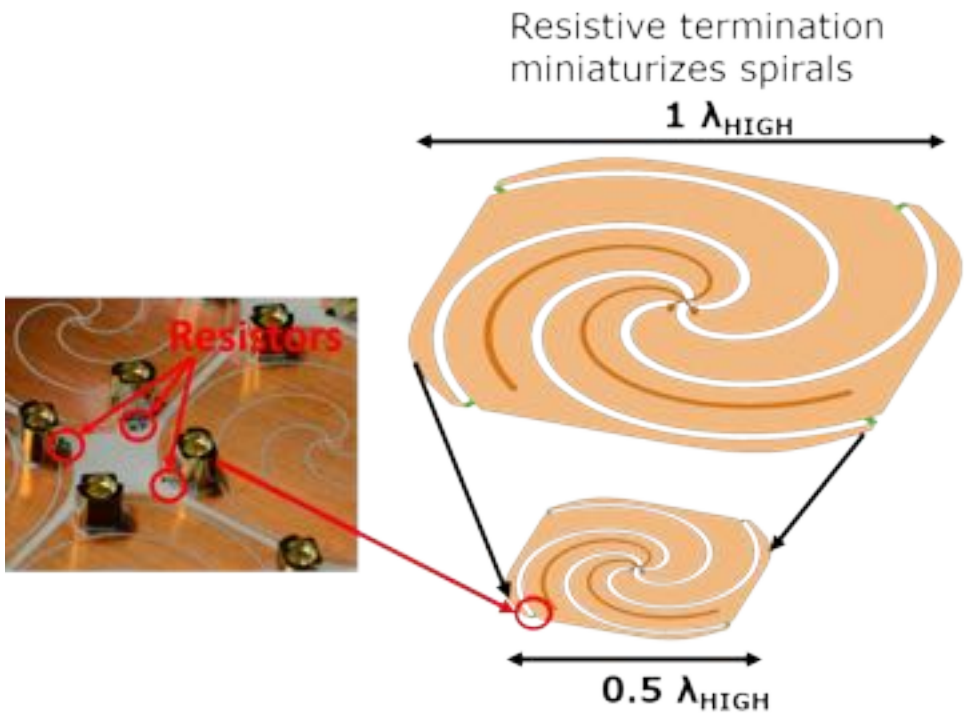

Figure 14 Resistive terminations enable spiral miniaturization.

3.2 Miniaturized Spiral Element

To construct the four-arm spiral array, each spiral element was placed in a 45.7 mm × 45.7 mm unit cell. The spiral arms are constant width slots etched into a rounded square copper sheet. The slot width was optimized for a good impedance match at the feed point and is equal to 0.54 mm. Also, each spiral arm was of the Archimedean type, where the slot's center curve followed the path $r = a\varphi$, where r is the radius, φ is the angle, and a is the growth rate (3.24 mm/rad). A single surface mount resistor (100 Ω, 0402 size) was soldered across the slot at the end of each spiral arm.

The spiral was etched on the bottom layer of a 2-layer printed circuit board (PCB) with the balun on the top layer (RO4350B, ½ oz. Cu, 10 mil thick, $\varepsilon r = 3.48$, $\tan\delta = 0.003$). The cross section of the spiral element is shown below. As depicted, a microstrip

infinite balun was used to accomplish two goals [88]. It provided a balanced excitation that matched to the 50 Ω coaxial feed impedance. The microstrip width was tapered (0.38 mm to 0.11 mm) to reach an impedance of approximately 130 Ω at the center of the spiral. Each microstrip was fed with a 50 Ω MMCX connector soldered at the spiral arms. This connector snapped onto an MMCX-MMCX adapter to keep the ground plane height constant. Below the ground plane, the MMCX adapter connected to another MMCX-SMA adapter for measurements. This approach considerably reduced assembly time and enabled a more robust and modular design. Ferrite cores were placed around the coax adapters to suppress residual currents on the shielding. Finally, the array was backed by a metal ground plane at a distance of $\lambda_{LOW}/16$ or 11.4 mm, where λ_{LOW} is the wavelength at the lowest frequency of operation. It is noted that care must be taken into account to ensure a symmetric antenna structure. Notably, slight asymmetries in soldering or assembly can significantly affect Tx/Rx isolation.

Full wave simulations of the infinite spiral array demonstrated a port-to-port isolation of 35 dB across 1.5-4.5 GHz (3:1 bandwidth). The active VSWR was <2, even when scanning. The realized gain maintained acceptable values when scanning. A 1×5 semi-infinite array simulation produced similar results across the same bandwidth.

3.3 Design and Fabrication

The details of the proposed four-arm spiral. As seen, a pair of arms is used for Tx and the other pair for Rx [38]. It is essential that both arm pairs are of high symmetry to ensure balancing of the signal phase and therefore improve Tx/Rx isolation. To accomplish this, it is necessary that the spiral arms and feeds are symmetric. In our case,

only two spiral arms require coaxial cable feeds, one for Tx and the other for Rx. Therefore, dummy coaxial cables were added to maintain symmetry. Measurements with dummy cables showed about 10 dB additional Tx/Rx isolation.

The proposed four-arm spiral relies on physical symmetry to produce high isolation. Thus, creating a symmetric spiral, including its balun, is of great importance, especially at the upper frequencies of operation where physical dimensions are electrically larger. For our case, we modified the two-arm spiral infinite balun [88] for adaptation in our four-arm spirals. Our challenge is the center feeding of each pair of spirals. For our case, balun symmetry was assured by routing one of the two microstrip feeds through a via. This enabled balun placement on a single layer of the PCB, simplifying the fabrication process.

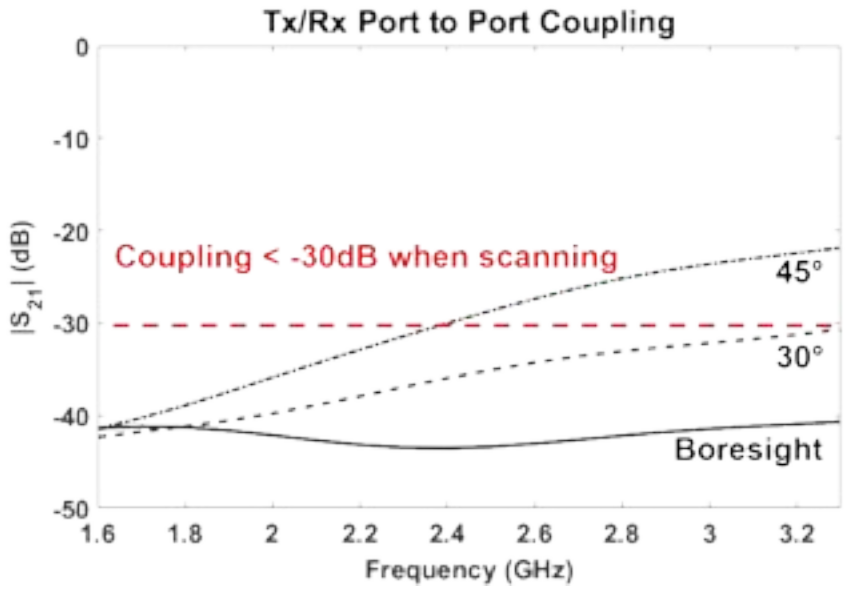

Figure 15 Wideband Tx/Rx isolation is achieved when scanning. Note that the simulated isolation of the infinite array remains high across 1.6-3.28 GHz when scanning to 30°.

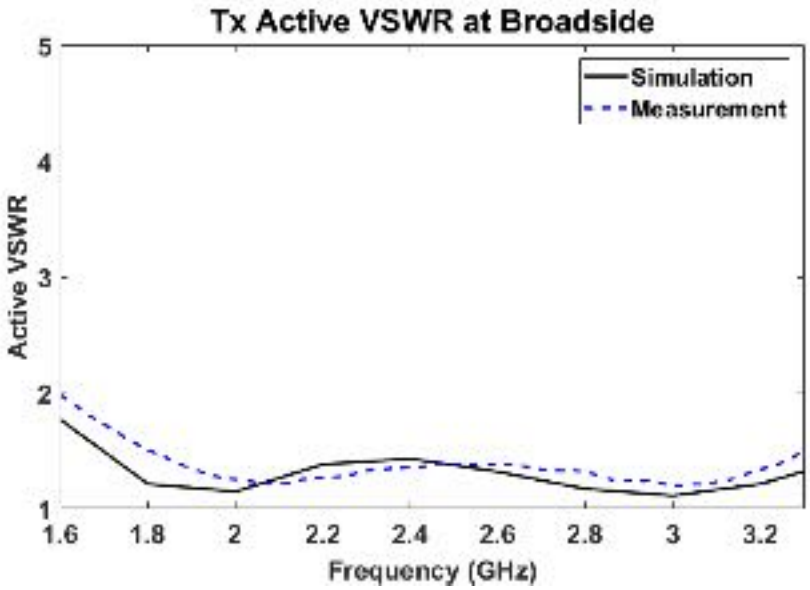

Figure 16 Measured Tx active VSWR in the center element of the 5×5 array agreed well with simulation and was <2 across the entire bandwidth at broadside. As expected due to symmetry, this was also the case for Rx (not shown).

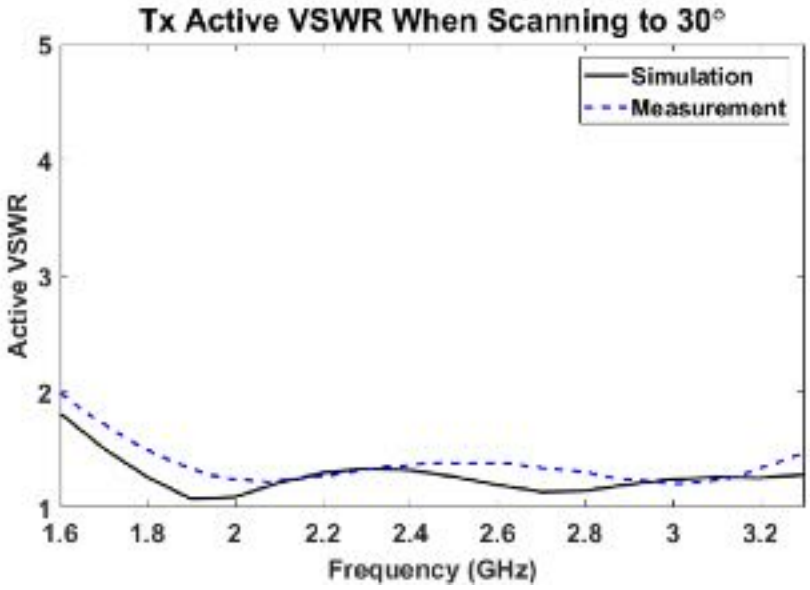

Figure 17 Measured Tx active VSWR at the center element in the 5×5 array matched simulations well when scanning to 30° and never exceeded 2.5 across 1.6-3.28 GHz.

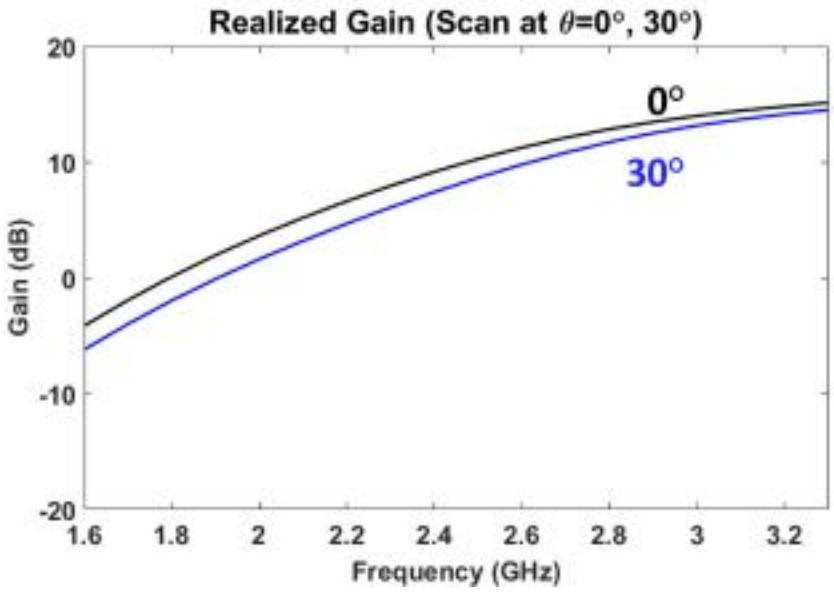

Figure 18 Simulated realized gain at broadside and scanning θ to 30°.

Alternatively, an investigation into a three-layer design, where each balun's microstrip is placed on a separate layer, did not lead to as high isolation at the higher frequencies. The four-arm spiral used a careful cross-over of the excitation to ensure symmetry. Foam structural supports were also placed between the antenna PCB and ground plane for added mechanical stability without adversely affecting the measured isolation [89].

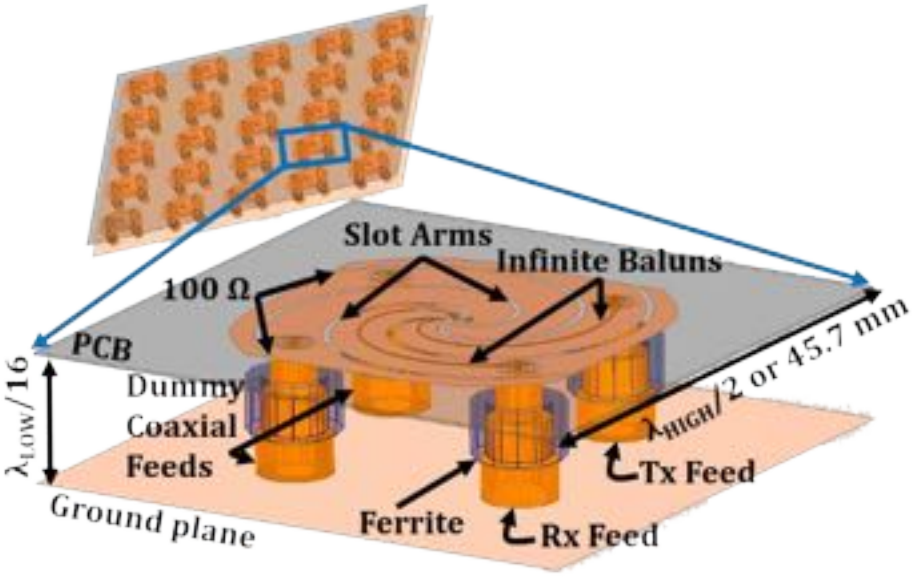

Figure 19 Prototype 5×5 array showing the design of the Tx/Rx four-arm spiral element.

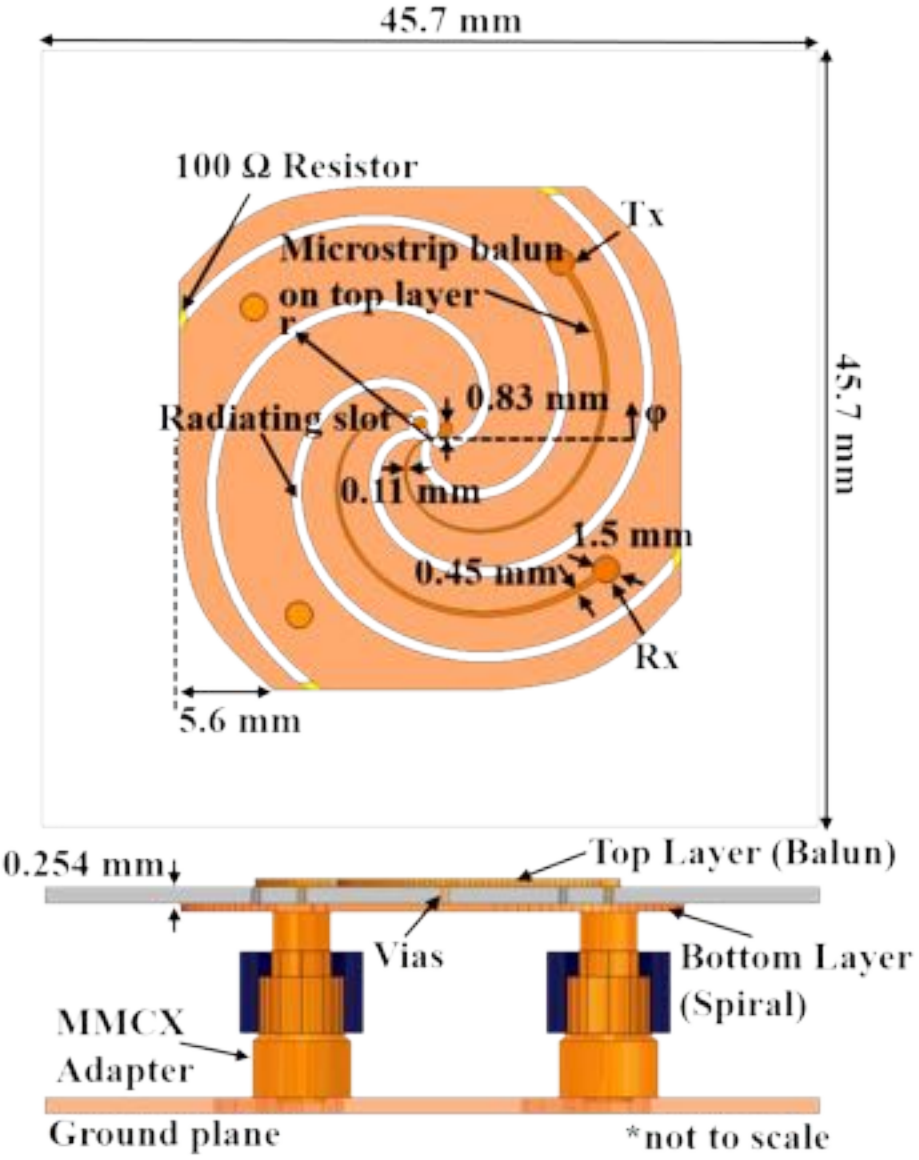

Figure 20 Dimensions of the four-arm spiral unit cell (top and bottom are the spiral aperture and cross section respectively). Notably, the balun was placed on the top layer with the spiral on the bottom layer.

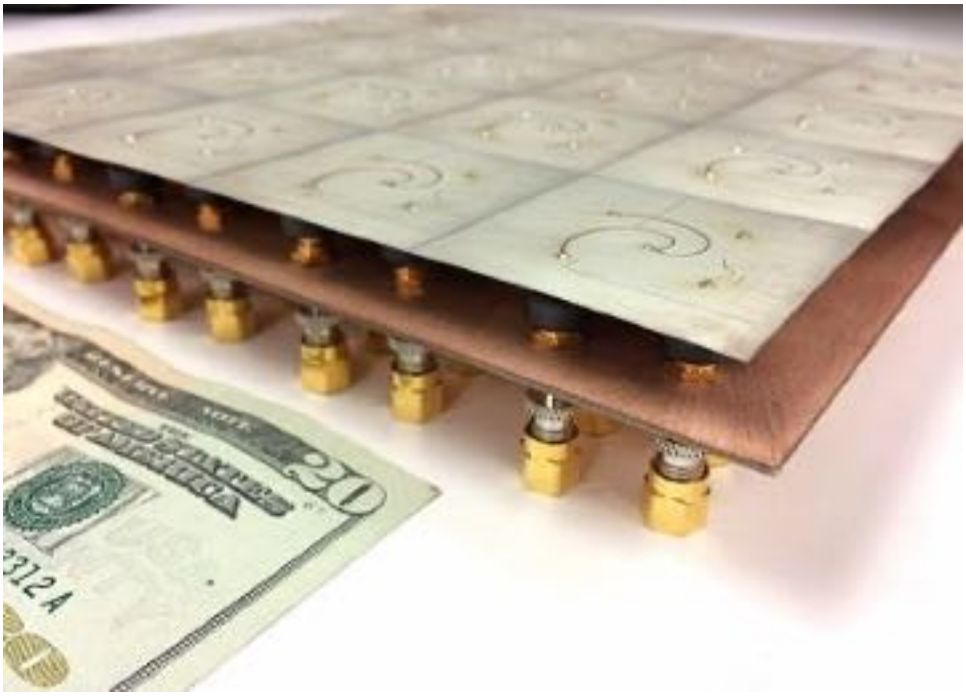

Figure 21 Photo of the fabricated 5×5 array.

3.4 S-Parameter and Pattern Measurements

VSWR and Tx/Rx port-to-port isolation were measured with a Vector Network Analyzer (VNA). The MMCX adapters were not de-embedded from the measurements and all unused ports were terminated with 50 Ω. The active VSWR at the Tx and Rx ports was <2 across the entire bandwidth at broadside. No appreciable degradation was observed in active VSWR when scanning. The Tx/Rx port-to-port coupling ($|S21|^2$) was measured at the Tx and Rx SMA connectors. Measurements confirmed simulations and showed 35 dB Tx/Rx isolation at the worst case at the center of the 5×5 array. When scanning down to 30°, the isolation was reduced by only 3 dB at the worst case. The measured gain patterns matched simulation fairly well.

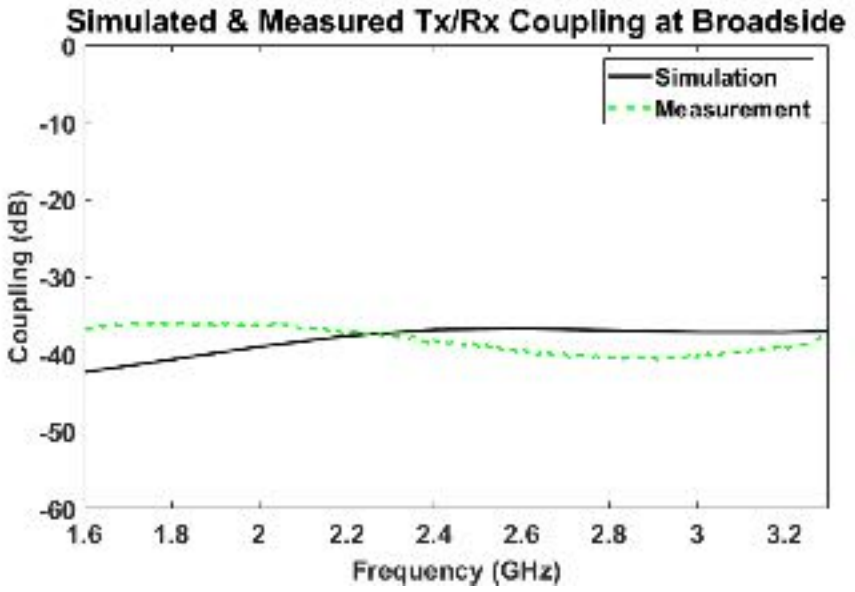

Figure 22 Simulated and measured Tx active coupling at the center Rx element vs simulations, showing a minimum of 35 dB isolation.

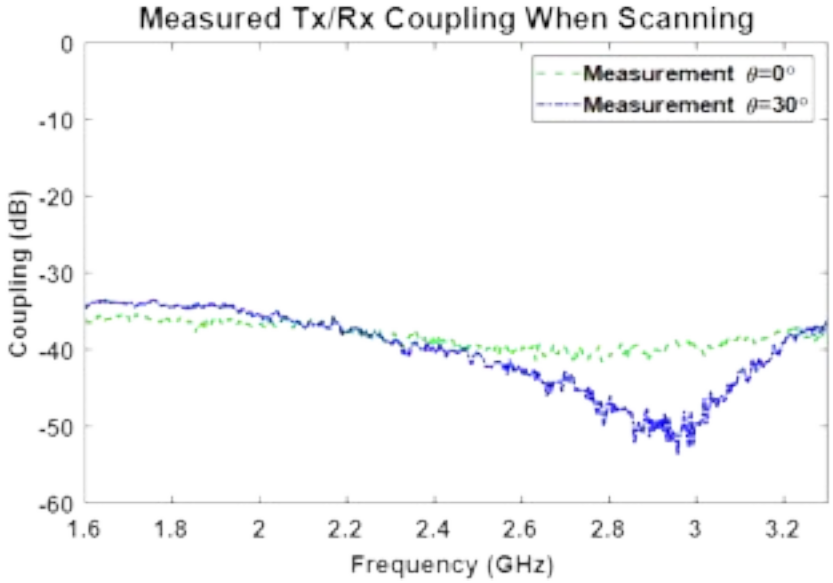

Figure 23 Measured active coupling of the center Rx spiral within the 5×5 array. Scanning at θ = 30 reduced isolation by only 3 dB as compared with broadside. Isolation is measured to be 35 dB at broadside across 1.6-3.28 GHz.

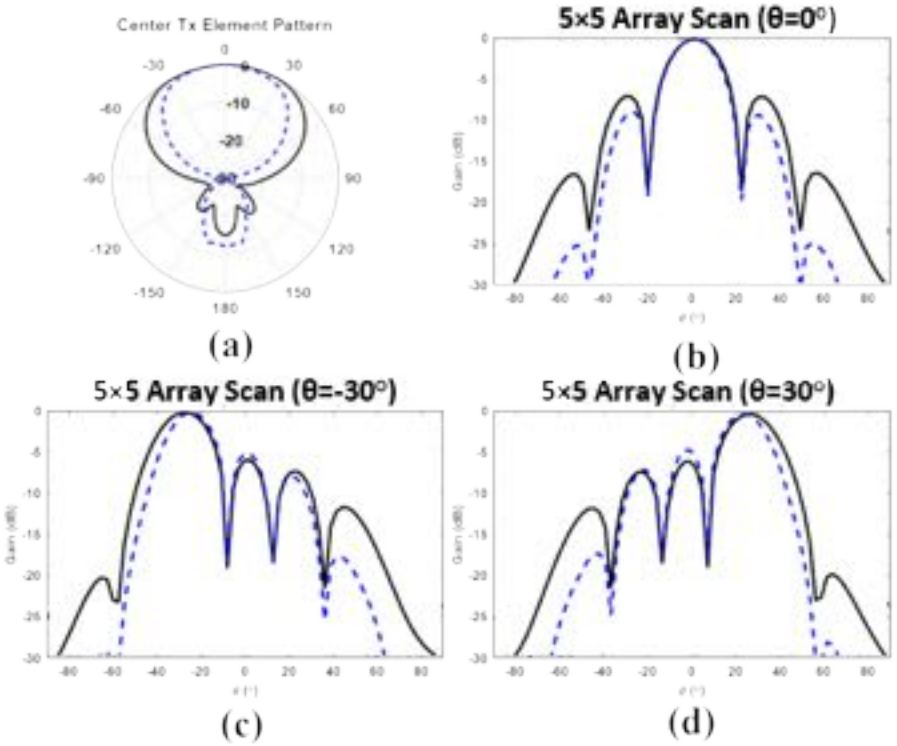

Figure 24 Simulated and measured normalized Tx array gain pattern for a 5×5 spiral array. (a) single element pattern of the center element, (b) array pattern at 0°, (c) array pattern at -30°, and (d) array pattern 30°. Simulations and measurements are shown in solid and dashed lines, respectively.

3.5 Mutual Element Coupling Requirements with Power Amplifier Noise

A component of the Tx self-interference is thermal noise, which becomes a challenge as the power amplifier's (PA) noise figure (NF) rises. This noise from the transmitter couples to the receiver increasing its noise figure. The receiver noise level affects the signal to noise ratio (SNR), determining the maximum data rate. By measuring

the mutual coupling between the transmit and receive ports, we can calculate noise at the receiver. The schematic for a radio with a single Tx and Rx is shown below.

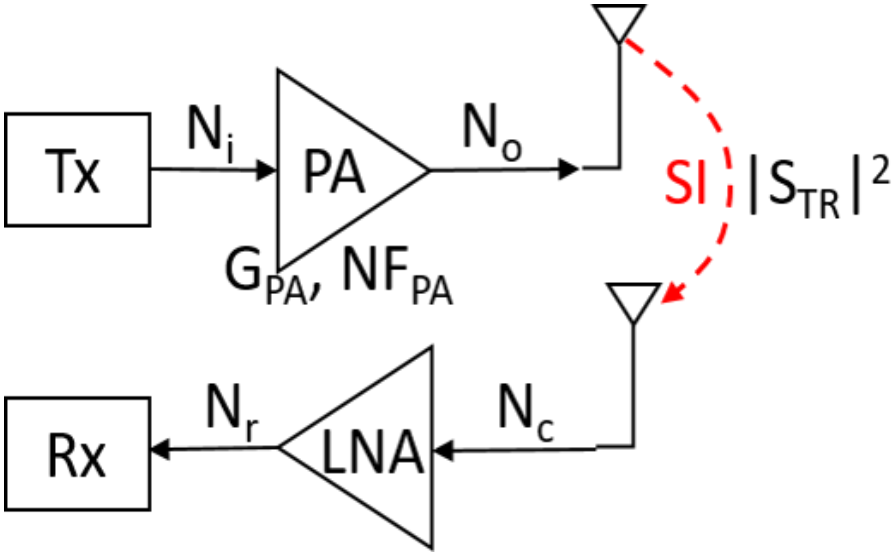

Figure 25 Schematic for a single element of the transmit and receive chain used to determine the total interference power at the receiver.

The transmit output noise, N_o, is the input noise, N_i, times the gain, G_{PA}, times the noise figure NF_{PA}. The noise at the receiver due to the PA, N_c, is given below.

$$N_c = G_{PA}F_{PA}N_i \times |S_{T,R}|^2, \quad (1)$$

The required level of isolation to make the coupled noise power equal to the input noise is a function of the PA's gain and noise factor (F).

$$|S_{T,R}|^2 = \frac{1}{G_{PA}F_{PA}}, \quad (2)$$

Extending this to an array, by superposition, the total noise received is the sum of all coupled noises.

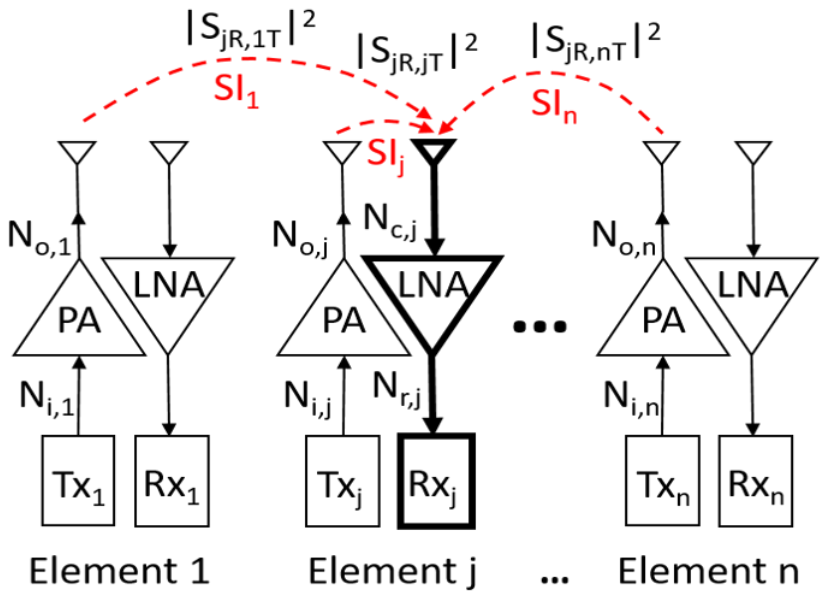

Figure 26 Schematic extended to an array.

If the component performance is identical for N elements, the required coupling is 1/N times the single element coupled noise as shown below.

$$N_c = \sum_{k=1}^{N} G_{PA,k} F_{PA,k} N_i \left|S_{jR,kT}\right|^2, \tag{3}$$

$$\left|S_{R,T}\right|^2 = \frac{1}{N \times G_{PA} \times F_{PA}}, \tag{4}$$

The heat map below shows the Tx to Rx mutual coupling to the center element. As can be seen, the adjacent eight elements contribute virtually all of the coupled noise power.

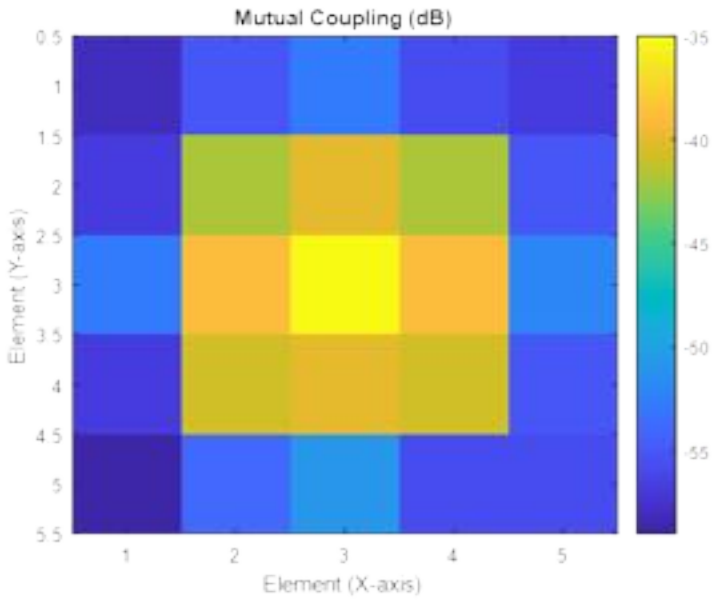

Figure 27 Heat map of the measured mutual coupling between adjacent element's transmit and the center receive port.

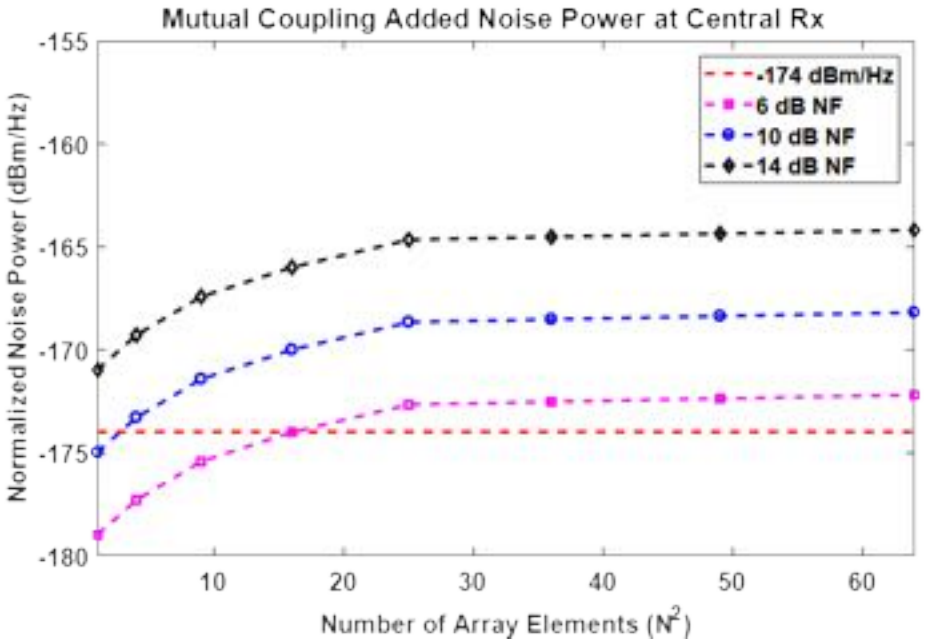

Figure 28 Noise increases as a function of array size. The fabricated array's coupling terms were used.

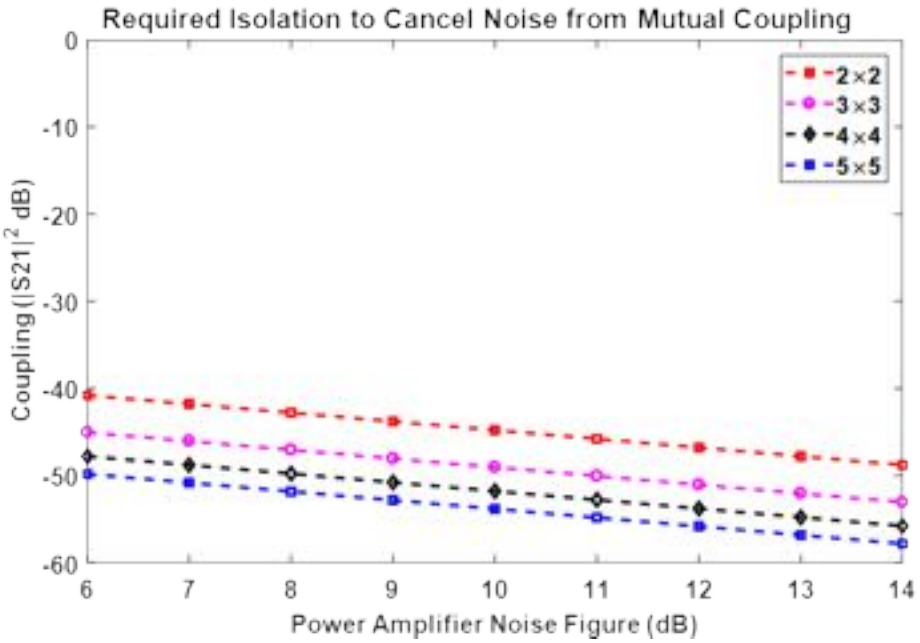

Figure 29 Required level of isolation for various array sizes to ensure the coupled noise is suppressed to the thermal noise floor.

Given an array size with identical mutual coupling, we would like to know what isolation is required to suppress the coupled noise to the thermal noise floor. The figure above shows isolation levels for various array sizes and noise figures. For example, in a 3×3 array with an 8 dB NF, the isolation should be at least 47 dB. However, it is not uncommon for power amplifiers to have noise figures of 12 dB or greater. In such cases, the isolation should approach 50 dB.

3.6 RF Self-Interference Cancellation Filter and Conclusion

To increase total SI cancellation of the system, an RF self-interference cancellation (RF-SIC) filter was designed and optimized. The filter taps the Tx SI signal and injects the inverse of the antenna's coupling transfer function into the receiver. The

antenna's coupling transfer function is first simulated and measured. It is critical to simulate the delay and taps using the measured values as small changes can affect the final isolation value. Finally, the SI is reduced through destructive interference. To do so, the filter contained two banks of 6-tap delay and attenuation sections. The length of each tap was optimized to account for time delay of the antenna coupling. The attenuator values were selected to mimic the mutual loss from the coupling. The substrate used was a Rogers TMM10 with a 1.55 mm thickness.

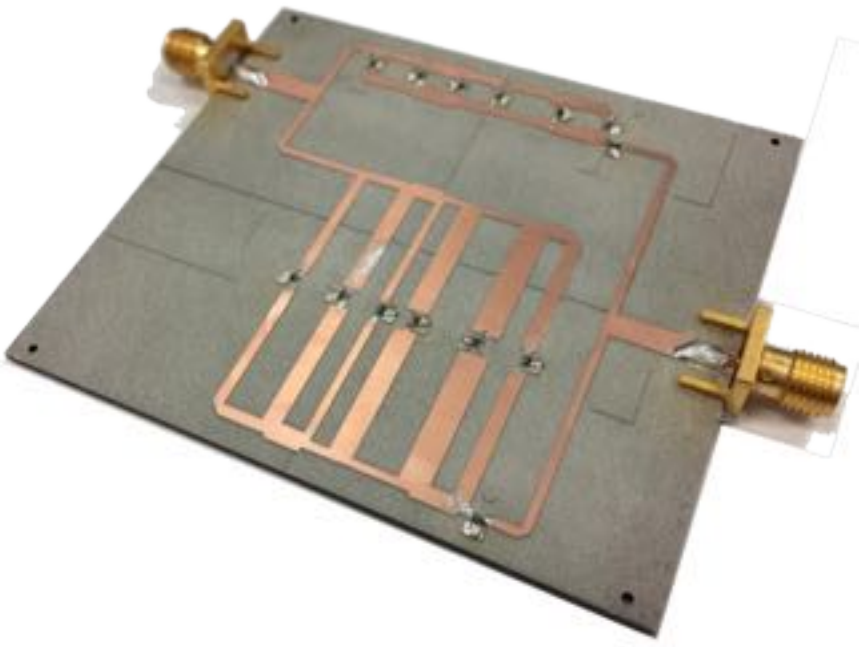

Figure 30 Photo of the RF-SIC filter after assembly and soldering.

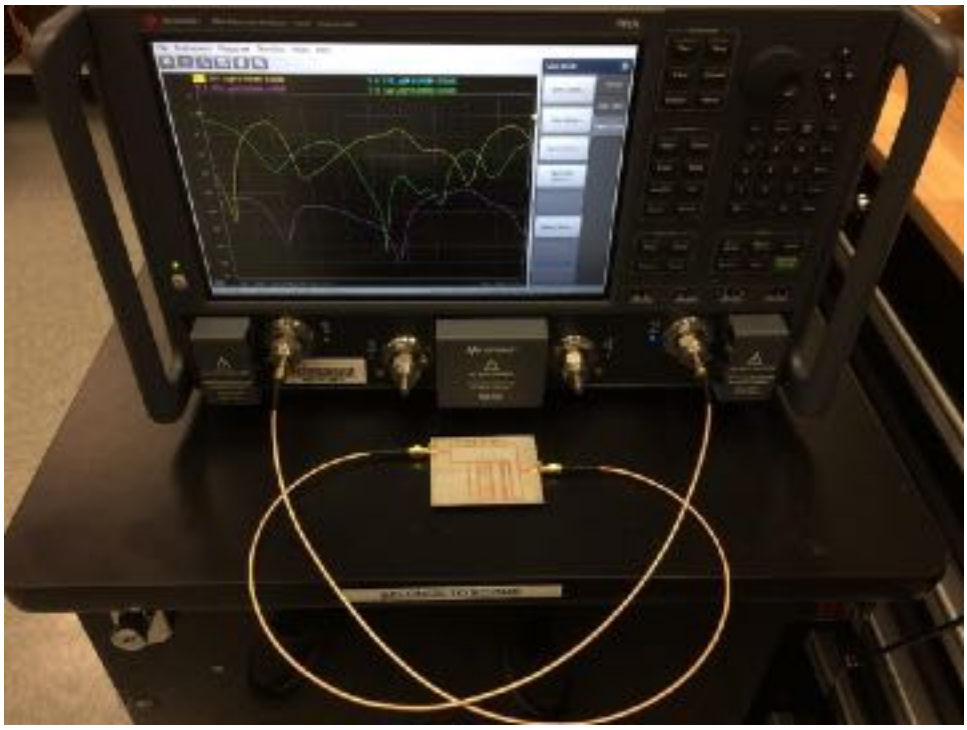

Figure 31 Photo of the RF-SIC filter under test with a vector network analyzer to determine its transfer function.

For the first time, we demonstrated a wideband array using four-arm spirals with high transmit-receive isolation for application in a Simultaneous Transmit and Receive (STAR) phased array. Array measurements showed 35 dB Tx/Rx isolation at the worst case across a 2:1 instantaneous bandwidth. A 5×5 prototype operating across 1.6-3.28 GHz was measured and results showed excellent agreement with simulation.

CHAPTER 4: ACTIVE STAR ANTENNA – TUNABLE BALUN TO IMPROVE ISOLATION

4.1 Passive STAR Antenna Limitations

As noted, the cancellation techniques of passive antennas stages designed for printed circuit boards (PCBs) were limited to ~35-40dB. But even more importantly, they required additional stages, such as external, bulky, or expensive beamformers to reinforce antenna stage cancellation. Critically, they relied on a high degree of symmetry and manufacturing precision, making them somewhat impractical. Additionally, to obtain marginally better isolation, substrates with low loss tangents were also used. These materials, such as PTFE, are impractical for fabrication and considerably more expensive than the ubiquitous FR-4. Despite their high frequency benefits, their cost is prohibitive to manufacture on a massive scale. Regardless, realistic balun fabrications, as will be demonstrated, introduce feed asymmetries that weaken isolation.

Our aim is to correct electrical asymmetries by incorporating tuning at the antenna cancellation stage. Additionally, this does not preclude self-interference cancellation (SIC) beamformers and circuits behind the antenna. Here, we demonstrate that 1) geometric and 2) excitation symmetries are necessary to achieve high isolation. For the first time, we propose strong transmit/receive isolation by integrating a chip into the antenna feed. The chip regulates the small amplitude imbalances causing this isolation degradation among the collocated antennas.

In this chapter, we discuss the design and simulation of a passive antenna whose cancellation method is based on symmetry and balanced feeding. Later, we examine the

isolation deterioration induced through asymmetry and the passive prototype's fabrication and measurements. Finally, we compare this design to the fabrication and measurement of an identical antenna with the active feed tuning. This active feed recoups the isolation lost from unpredictable fabrication effects, which is critical for practical antennas in STAR radios.

To focus on improving a single element's Tx/Rx isolation, we selected a previous single-element design with good passive isolation across wide bandwidths. This antenna was presented in [90] and extended in [50] with the fabrication of a modified concept. The model, shown below, consists of a vertical transmit monopole centered in a receive ring antenna.

It consists of a pair of half rings placed around a vertical monopole at the center. The monopole radiates vertical polarization. By contrast, the half rings radiate a horizontally polarized field. Notably, isolation was achieved by physical symmetry, balanced feeding, and the use of orthogonal polarization across the two antennas. Each half ring antenna was fed by a Marchand balun [91] fabricated on a printed circuit board (PCB). It is also important to note that the half rings were fed at 180° with respect to each other. This ensured the ring's pattern was similar to the monopole's omnidirectional pattern. That is, the half rings were used instead of a 1λ loop to avoid dissimilar Tx/Rx patterns and narrow bandwidths. This is critical for point-to-point radio links where the transmitted and received signals needs to be pointed in the same direction.

Notably, the antenna pair operates across 1.5-3 GHz (2:1 bandwidth). The monopole's large bandwidth is due to the flare's width and curvature. The flare's curve in the lower half of the antenna follows a semicircle, with a diameter equal to the

monopole's width. The monopole was fed by a 50 Ω SMA connector soldered to the ground plane. The SMA's pin was soldered to the single-sided copper face on the monopole board. The dimensions used in simulation are in terms of $\lambda_{LOW} = \lambda_{1.5GHz}$ = 20 cm. The ring's outer diameter was $\lambda_{LOW}/1.4$ and the monopole's height was $\lambda_{LOW}/5$. Also, the ring's width was $\lambda_{LOW}/14$. We note that the ring's high frequency operation was limited by the appearance of multiple lobes around 3 GHz despite having a matched input impedance (VSWR < 2).

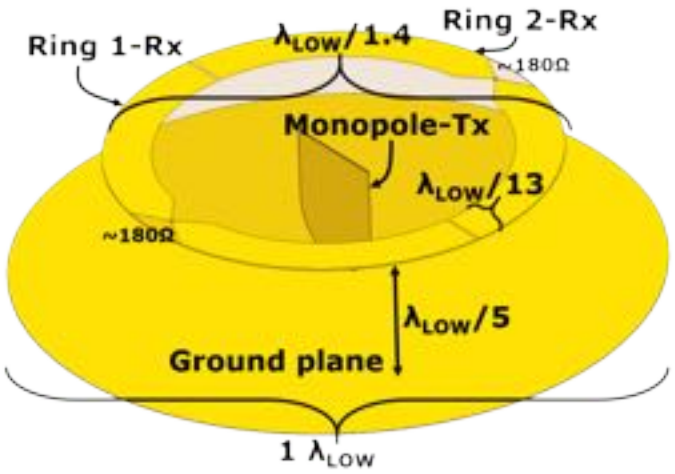

Figure 32 Antenna model with ideal feeds.

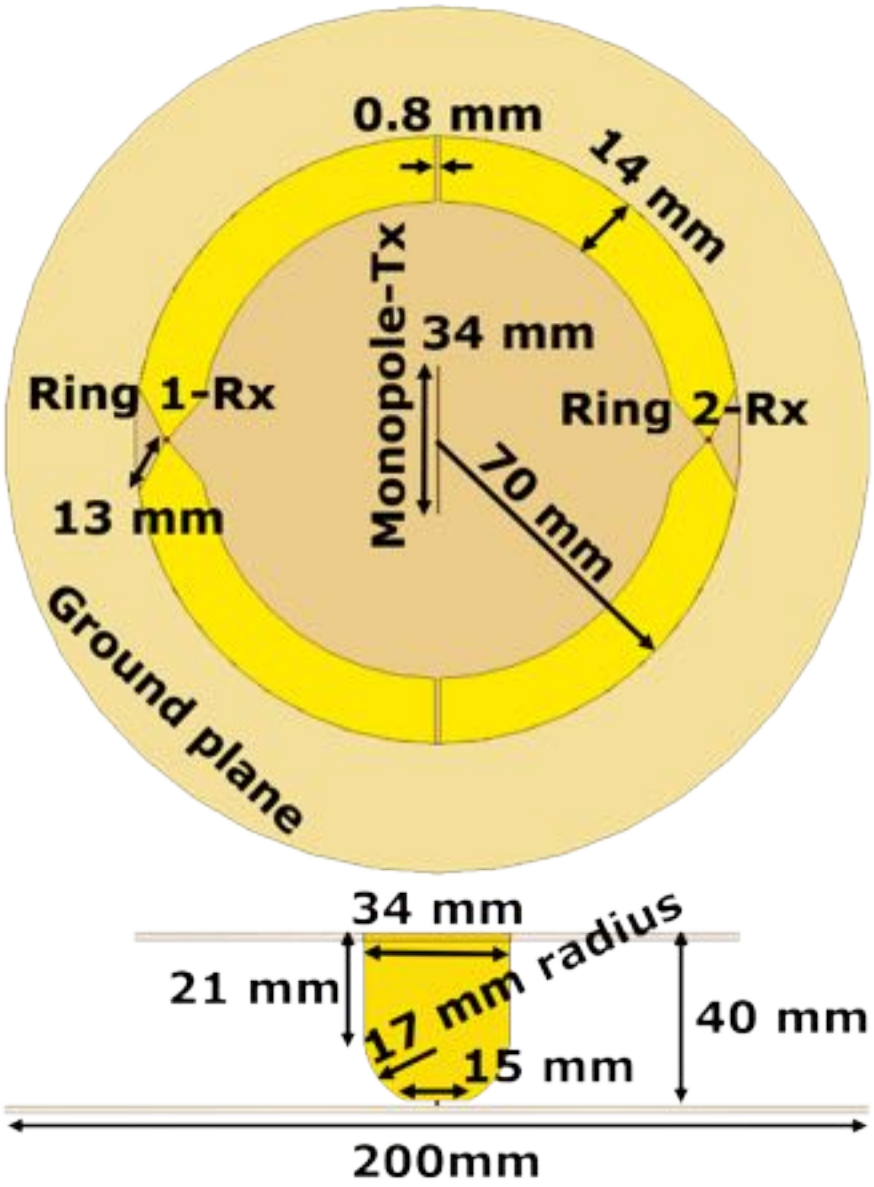

Figure 33 Diagram depicting the antenna's dimensions. A top down view is shown with its cross-section below.

Full-wave simulations showed excellent isolation that was greater than 60 dB across the entire operating bandwidth with good matching as well. Interestingly, the low frequency isolation increases due to the extreme symmetry

when the structure is electrically small. The radiation pattern cuts showed good omnidirectional shapes across broad bandwidths.

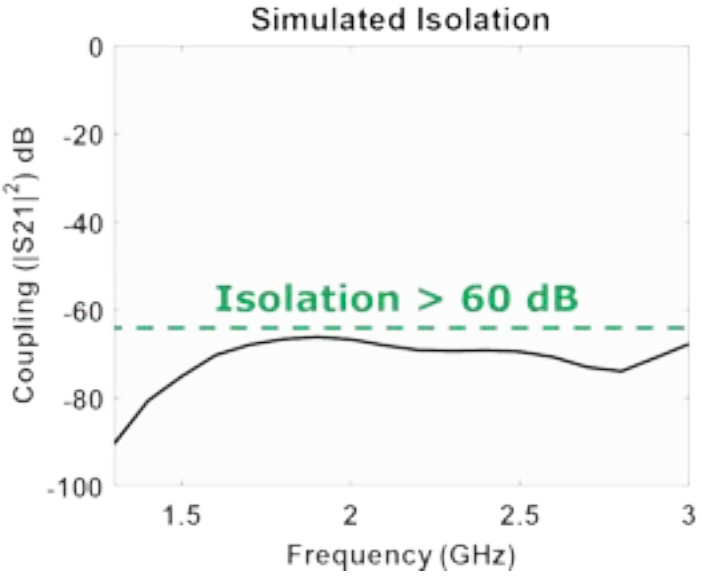

Figure 34 Full wave simulations with a perfect feed and symmetry for frequency independent high isolation.

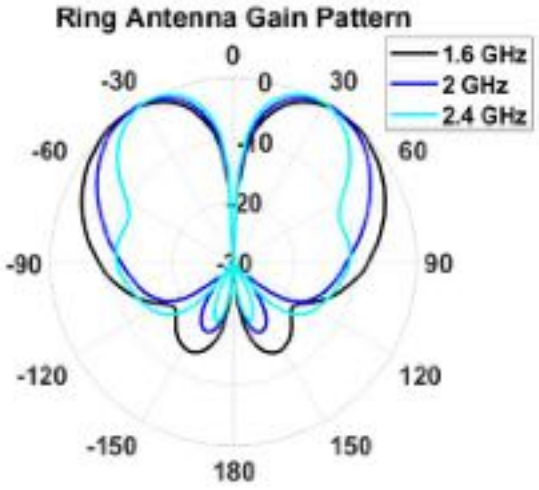

Figure 35 Ring antenna pattern at different frequencies.

To ensure good Tx/Rx isolation in the antenna, the radiating structure must self-cancel the transmit signal. As such, symmetry and precisely balanced feeding are critical to achieving high isolation. For symmetric elements to do so, they must be fed with a balanced feed. To ensure good balun output characteristics, simulations report the amplitude and phase of each arm relative to the input ground plane. Specifically, the goal for the balun arm's outputs is to be equal in amplitude and 180° out of phase.

Several PCB baluns for ultra-wideband arrays exist, notably the Marchand balun. It is a compact balun, with dimensions as small as $\lambda/20$, and produces good antipodal feeding for use in 9:1 bandwidth arrays. Additionally, it can provide 3:1 or greater impedance transformations, as in the case of the tightly coupled dipole array.

In the ring/monopole antenna, the ring is fed with a wideband balun. Originally, one such device was the Marchand balun. To determine this balun's capability in a STAR antenna, we simulated it in a full-wave electromagnetic simulator. Notably, while the amplitude and phase with respect to frequency were reasonable, they did not achieve the precision required for STAR. Additionally, the best performing frequencies for amplitude and phase differed. This implies low isolation across the entire bandwidth. Therefore, an alternative balun with greater balancing is attractive.

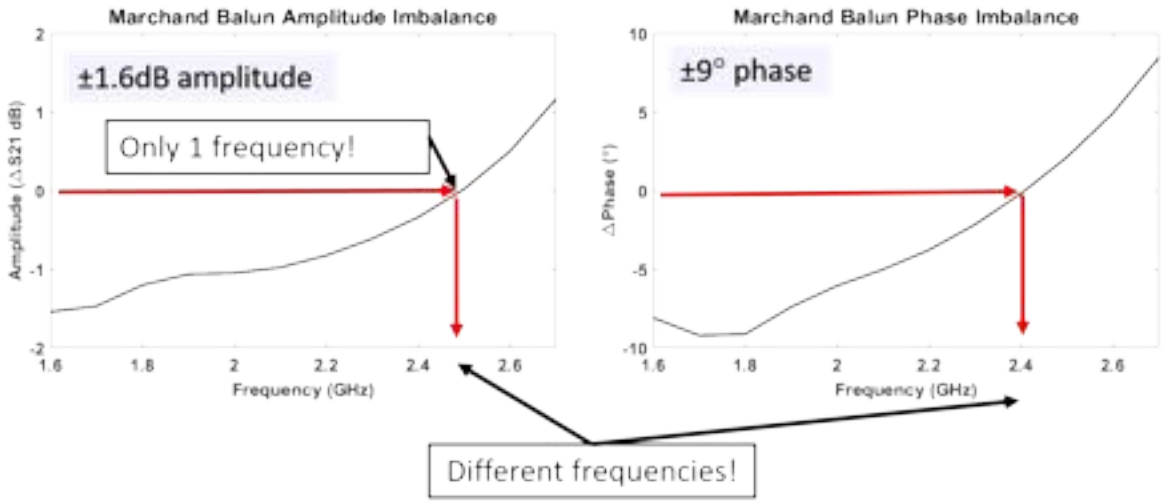

Figure 36 The Marchand balun suffers in wideband STAR applications due to amplitude and phase balancing at different frequencies.

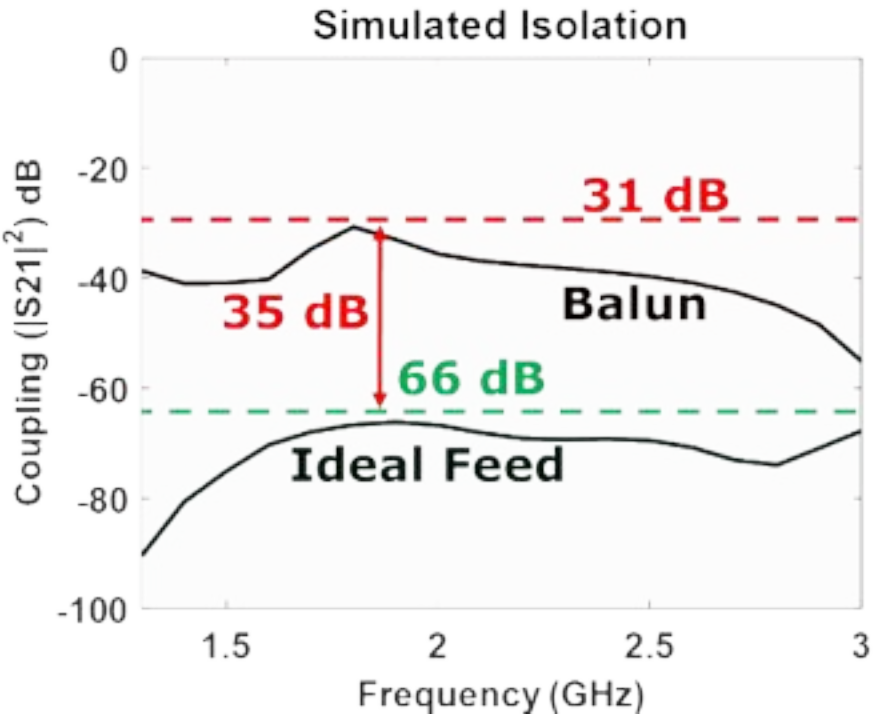

Figure 37 A realistic balun lowers isolation as compared with an ideal balun because of feed imbalances.

One such balun is the tapered microstrip feed. Like the Marchand balun, it also achieves a 3:1 or greater impedance transformation along with ultra-wideband operation. Although, achieving 9:1 bandwidths require a physically longer balun. In contrast, the tapered microstrip achieves wideband amplitude and phase matching, making this balun attractive for STAR. Additionally, smooth phase curves are beneficial for designing RF cancellation filters behind the antenna.

However, there still exists minute amplitude and phase imbalances at the microstrip balun's output. Further, even small fabrication and assembly tolerances impact these imbalances, affecting isolation. To determine an appropriate solution, we desired to measure these imbalances in a fabricated balun. However, this is difficult with current laboratory equipment as our vector network analyzer (VNA) ports are at 50 Ω and single-ended as compared to the 100 Ω differential feed.

To estimate the imbalances in a realistic prototype, we created a test with back to back baluns in two configurations. The estimated amplitude and phase imbalances can be extracted by post-processing the S-parameter measurements. The test results are significant because they specify the direction we should take to rectify the balun irregularities.

The two configurations are as follows. The first back to back balun is in the standard configuration where the signal and ground traces are connected. The second configuration is inverted, specifically, the signal trace of one balun is connected to the ground plane of the other. In an ideal balun, the difference between the S21 of these devices should be zero. However, because the prototypes' amplitude and phase imbalances, we expect to observe a non-zero difference. Put another way, half of the back

to back balun is identical in both scenarios, so we are measuring the effect of the inversion.

Two back to back baluns were fabricated and their S-parameters were measured with a VNA. Each balun PCB was 45 mm by 16 mm corresponding to λ/5 at the lowest frequency of operation. The substrate was 31 mil thick (0.787 mm) FR-4 (ε_R= 4.4) with 1 oz. copper cladding. The 50 Ω ends of each microstrip were fed with through hole SMA connectors.

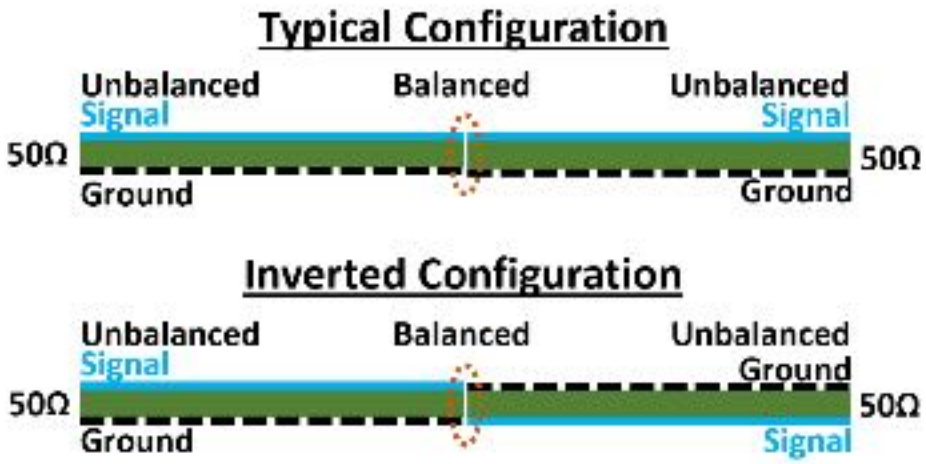

Figure 38 Back to back balun PCB stack up showing the typical and inverted signal/ground connections.

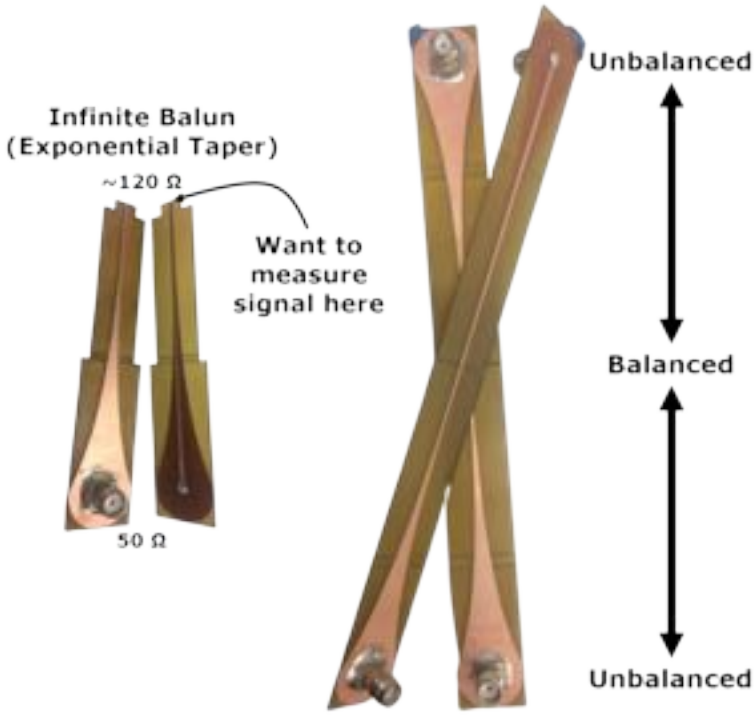

Figure 39 Photo of the balun for the passive matching prototype (left) and the corresponding back to back baluns (right).

Measurements indicated a ±0.4 dB range of amplitude imbalances across the ring/monopole antenna's bandwidth. The phase error was approximately 0.1° or less. This indicates fairly good phase alignment with room for improvement with amplitude. Therefore, we opted for amplitude tuning to regain electrical symmetry and high isolation.

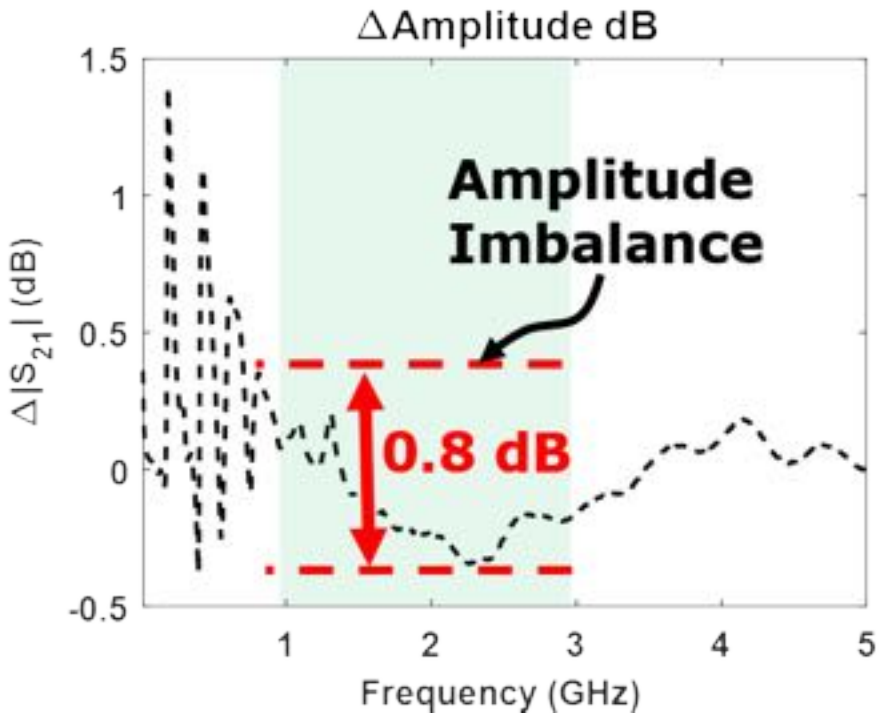

Figure 40 Amplitude imbalance measured from the back to back baluns.

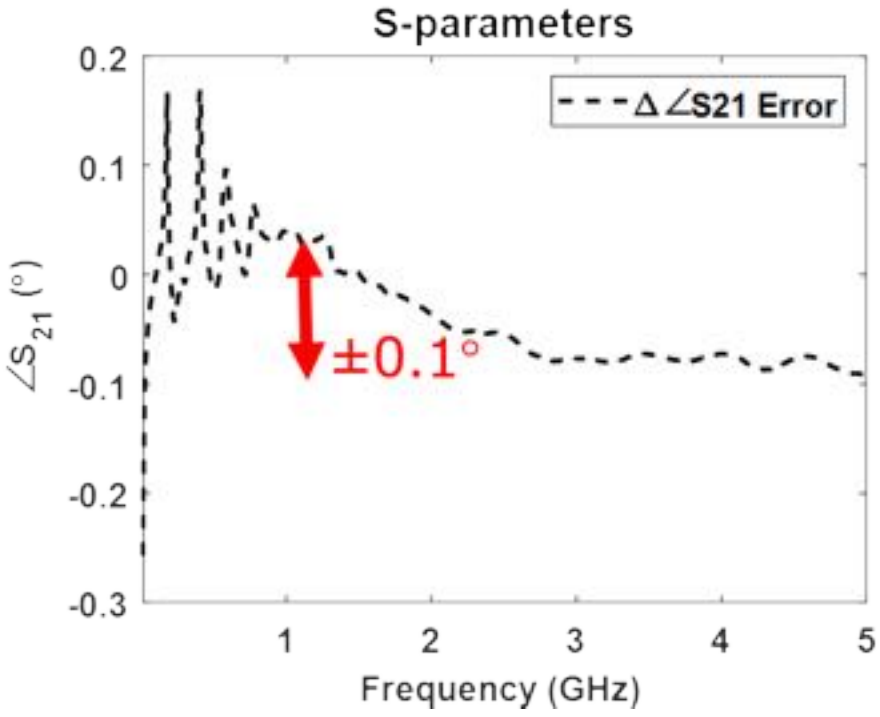

Figure 41 Phase imbalance measured from the back to back baluns.

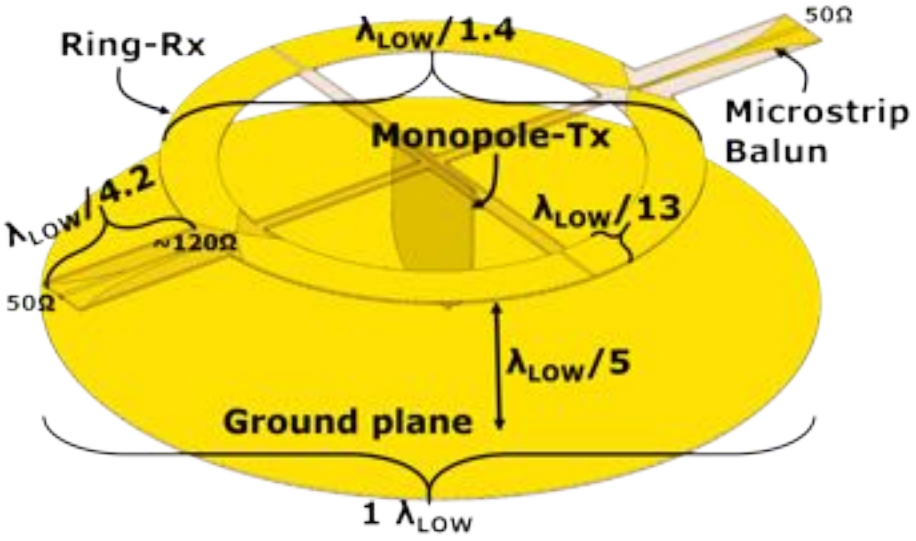

Figure 42 Addition of the microstrip balun lowered Tx/Rx isolation compared with ideal feed simulations.

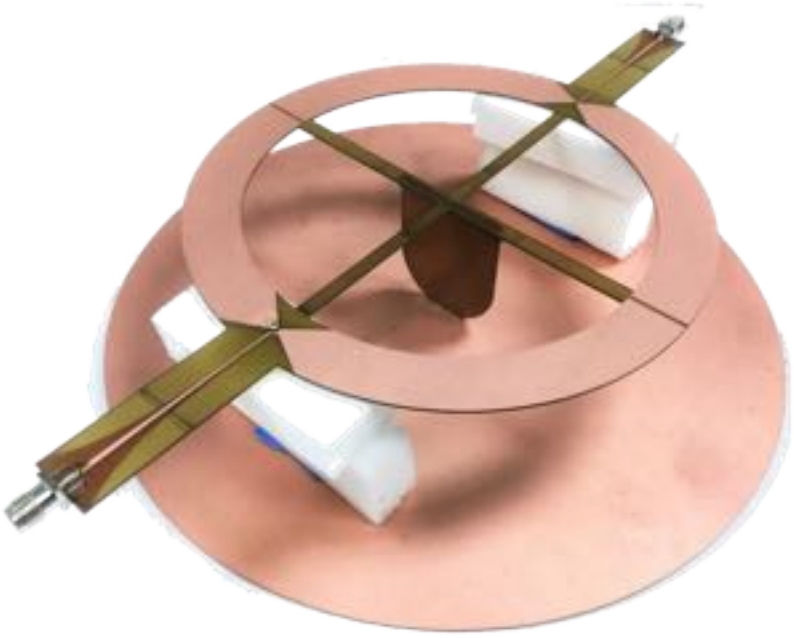

Figure 43 Photo of the fabricated prototype with passive matching.

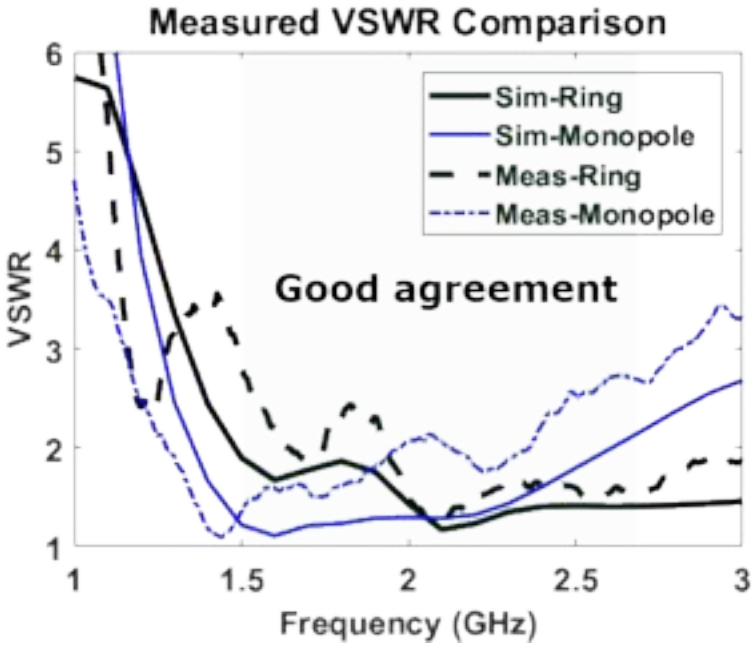

Figure 44 Passive measured and simulated VSWR for the Tx and Rx antennas.

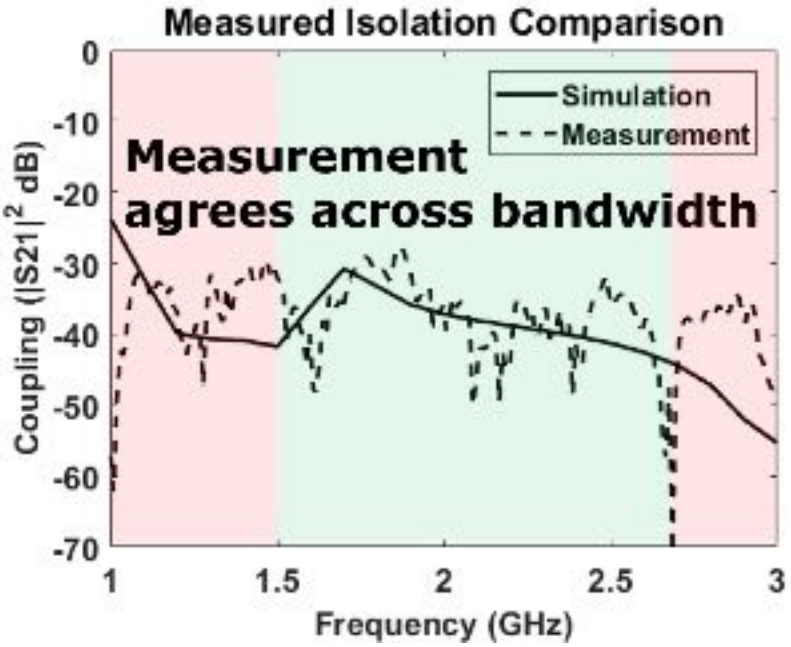

Figure 45 Passive prototype measured and simulated isolation curves agree well across the bandwidth of operation.

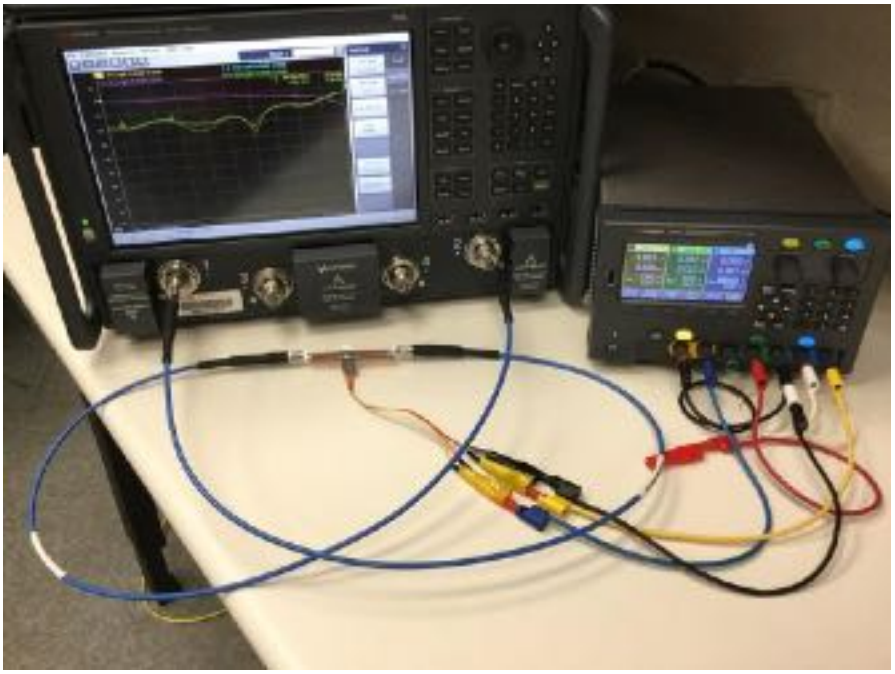

Figure 46 Test bed for the attenuator characterization circuit.

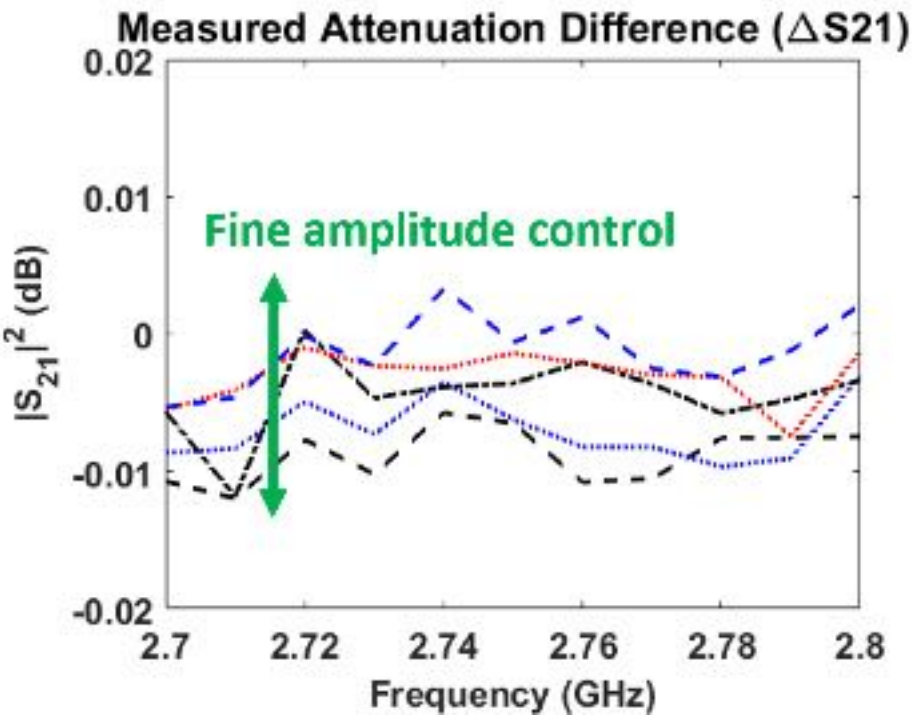

Figure 47 Analog attenuators demonstrate the fine control resolution.

4.2 Amplitude Tunable Balun to Improve Transmit Interference Cancellation

The aforementioned antenna was simulated and shown to deliver >60 dB isolation under ideal geometry conditions.

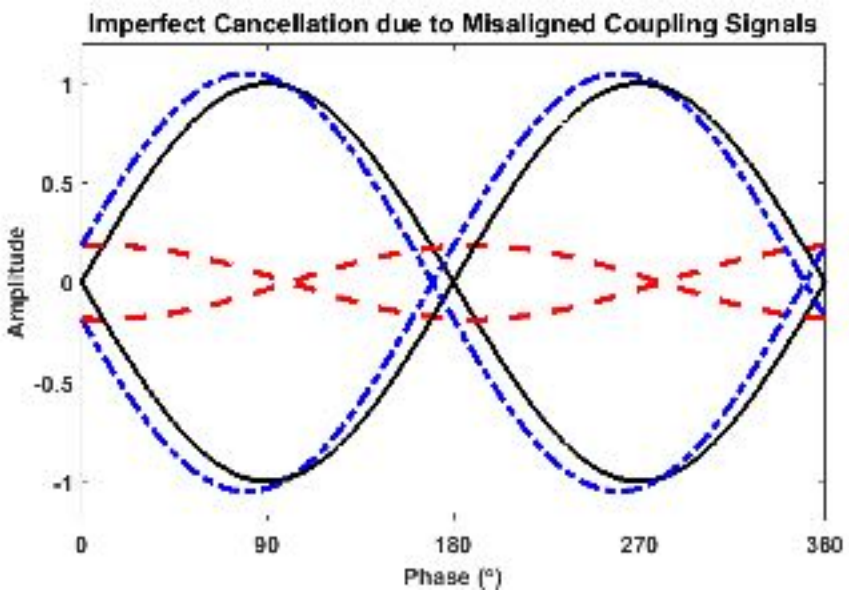

Figure 48 Misaligned signals lead to residual self-interference at the Rx port.

However, when a realistic balun was inserted, the isolation dropped to only 35 dB. Clearly, it is required to address this issue. In fact, to achieve high isolation, the balun outgoing and returning current density paths must have the following conditions:

- equal amplitude, and
- 180° phase difference.

However, the Marchand balun in [90] did not fulfill these requirements simultaneously, further reducing isolation. Additionally, the phase response was narrowband, limiting frequency tuning agility. Therefore, we resorted to a different balun with improved phase balance. One such balun on a PCB is the tapered microstrip feed. In simulation, we found that isolation worsened on FR-4 as compared with low loss tangent substrates. This was due to divergent current amplitudes in the balun arms. Therefore, amplitude correction is necessary to restore the two conditions for high isolation.

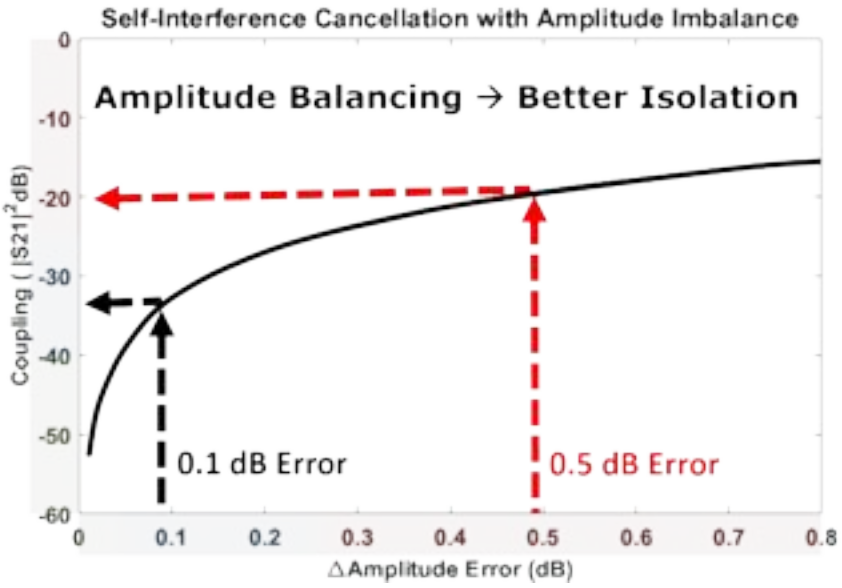

Figure 49 Better isolation is achieved with amplitude balancing. For example, to increase the isolation from 20 dB to 33 dB, the imbalance must decrease from 0.5 to 0.1 dB.

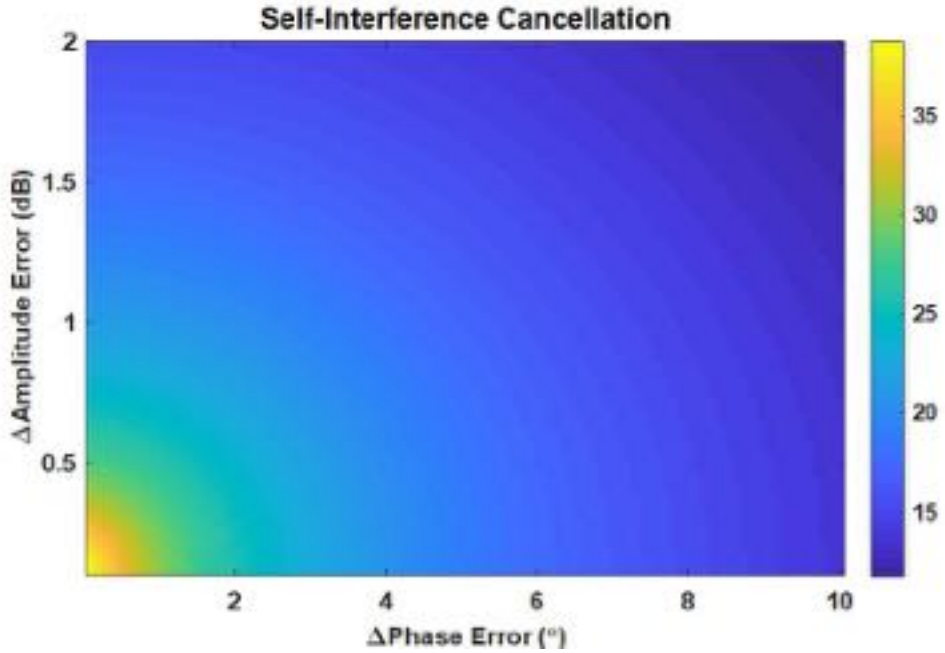

Figure 50 High isolation requires both amplitude and phase balancing. To ensure good isolation, phase errors must be less than 0.5°.

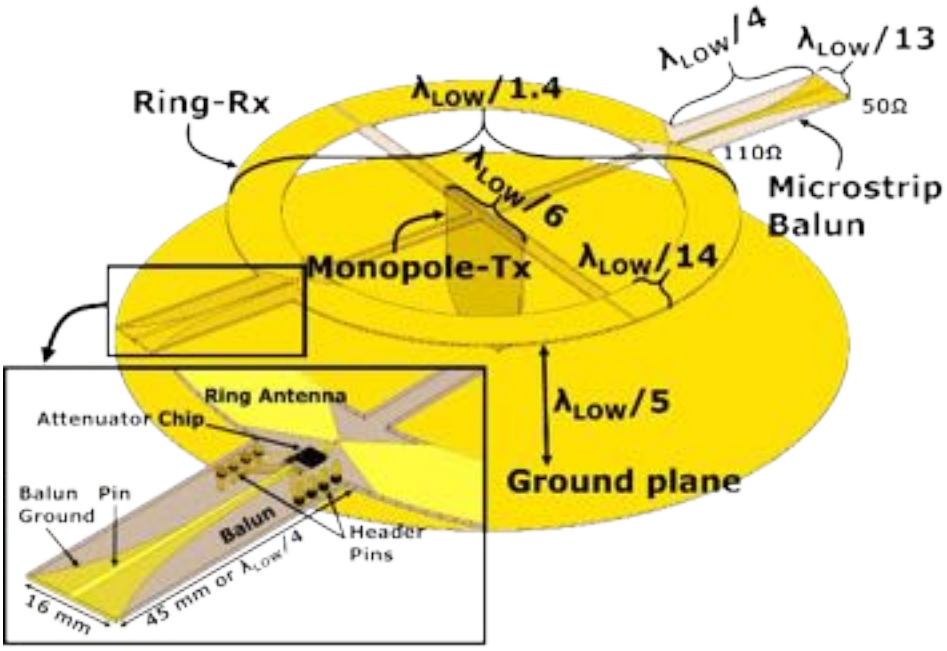

Figure 51 Dimensions of the passive prototype antenna with the tapered microstrip balun.

4.3 Antenna Design Details and Approach

The antenna was assembled from three stacked PCBs (31 mil or 0.787 mm thick FR-4, 1 oz. Cu). The boards were supported by press fit notches. Further, the center monopole supported the ring antenna and fixed its height above the ground plane. To enhance Tx/Rx coupling measurements, we ensured rigidity using light-weight foam blocks [89] inserted on opposite sides of the ring antenna. Subsequently, the SMA connectors on the monopole and ring were hand soldered.

4.4 Fabrication and Assembly

To improve antenna isolation in the presence of a practical balun, we used a microstrip balun using the proposed resistive control circuit. The goal is to adjust the feed's amplitude to ensure that the current densities at the antenna feed point are balanced. The ring antenna feed is an exponentially tapered microstrip transition to a differential line. But, current density imbalances exist between the microstrip ground plane and signal traces. As a result, isolation suffers. To correct it, we inserted an adjustable attenuator in the microstrip to achieve current density balance. The practical realization of this feed showed that ~0.2 dB difference existed between the positive (microstrip) and negative (return) lines of the current density when no resistor is inserted. The plot above shows the impact the current density imbalances on isolation.

We remark that digital attenuators limit the isolation to about 25 dB and are of no benefit in this case since the passive antenna already achieves greater isolation. This is because the fine attenuation increments required to achieve high isolation are less than the smallest step size of 0.25 dB. Therefore, we resorted to analog attenuators, where adjustments on the order of 0.05 dB can be realized.

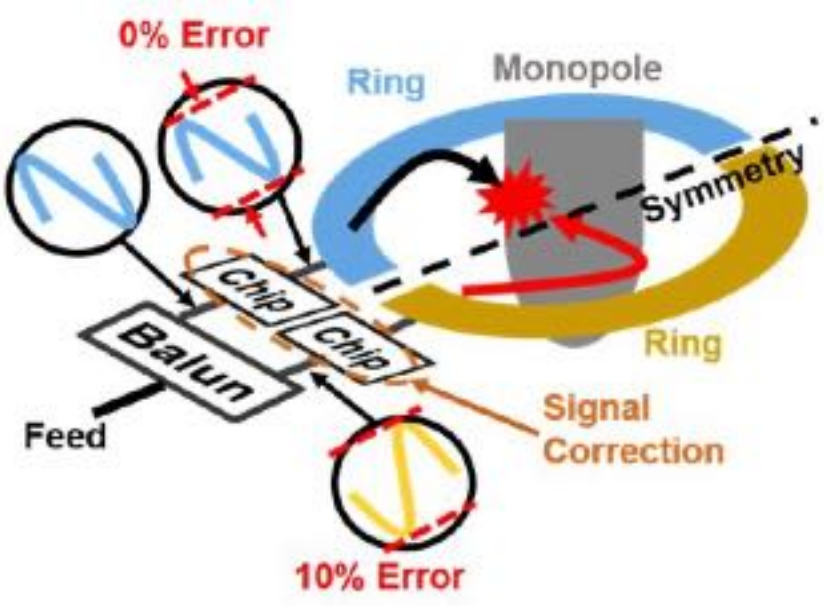

Figure 52 Tunable chip placed in the balun to increase Tx/Rx isolation by balancing the current densities on each balun arm.

The fabricated balun used an FR-4 substrate (31 mils thick, 1 oz. Cu) and had a length of about $\lambda_{LOW}/4$. To enable a good impedance match, an exponential taper of the form:

$$f(z) = \frac{w_1}{2} e^{-\frac{\ln(w_1/w_2)}{L}(z-z_0)}, \quad (5)$$

was used, where 2f(z) is the taper width and z is the fractional distance along the balun's length L. Also, w1 and w2 are the wide and narrow widths of the taper, respectively. Similarly, the microstrip ground plane used the same curve form as the signal line. Here, w1 = 1.6 mm and w2 = 0.6 mm for the signal trace. The ground plane's w1 = 16 mm and w2 = 0.6 mm. The parameter z0 is used to offset the balun from the coordinate system's origin. The PCB's size was 16×45 mm (width × length).

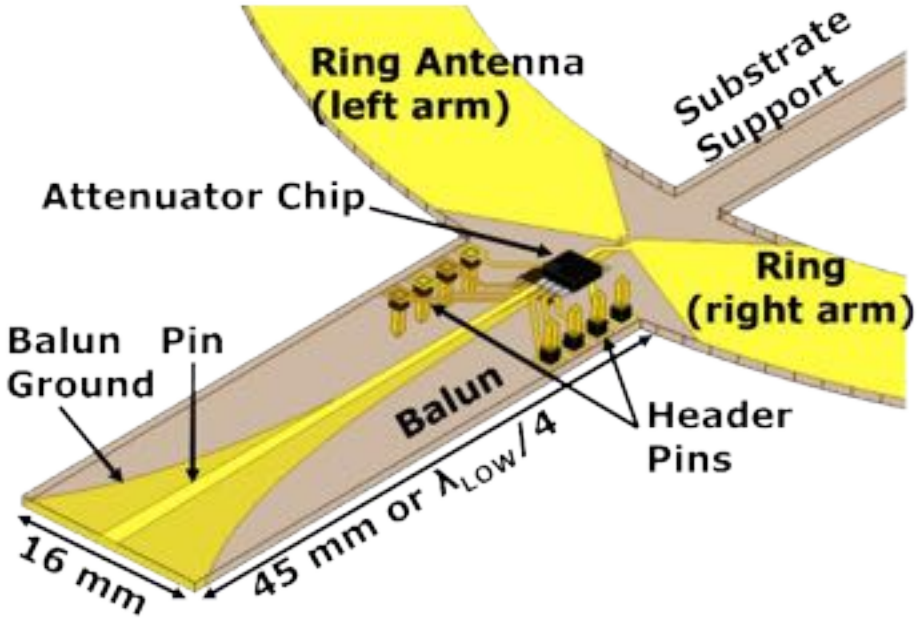

Figure 53 Attenuator chip inserted in the balun with analog amplitude control enables greater isolation than with just passive baluns. The chip's RF output attenuates the input signal by an amount controlled by the DC voltages from the header pins.

The device used to control the current density was a 0-8 GHz analog microwave attenuator with an attenuation range of 32 dB. Specifically, the component was a variable voltage attenuator in the thin shrink small-outline package (8-TSSOP) [92]. The chip's RF output was the input attenuated by a value determined from the control pin. The control pin's voltage range was -5 to 0 Volts. Attenuation increased as the voltage decreased to -5 V, with the attenuation increasing. Another pin tuned the input impedance. Both pins were used to tune the balun for the optimal Tx/Rx isolation. Critically, the chip exhibited a low phase shift across the frequency, specifically 0.9°±0.1° [92]. This 0.9° delay was unacceptable because it is approximately twice that of the passive balun's error. To correct this, two attenuators were inserted in each balun,

one for the signal trace and the other for the ground. Now, the difference between the chips' phase shifts canceled the 0.9° error, enabling phase matched tuning. Notably, the chip's worst case insertion loss was only 1.4 dB [92] at 2 GHz as compared to photonic systems that have >2 dB insertion losses at best [40].

4.5 Measurements and Conclusion

To achieve Tx/Rx isolation, we began changing the attenuation and impedance tuning values. The voltage on each pin was set with a digital power supply. In doing so, we found that an insertion difference of about 0.2 dB achieved the best isolation in our case. However, we remark that other solutions are possible. Importantly, measurements showed that we achieved 42 dB vs the 31 dB isolation without an insert. Notably, this 11 dB improvement is significant because, for the first time, it enables antennas fabricated on low-cost FR-4 to achieve greater Tx/Rx isolation than passive designs on low tanδ substrates. Also, the VSWR did not change appreciably while tuning. The large bandwidth of operation of 1.68-1.93 GHz (250 MHz bandwidth) is another key feature. This bandwidth is part of the Federal Communication Commission's (FCC) AWS-3 spectrum auction. We measured the antenna's Tx/Rx S-parameters with a vector network analyzer and radiation patterns in near-field anechoic chamber.

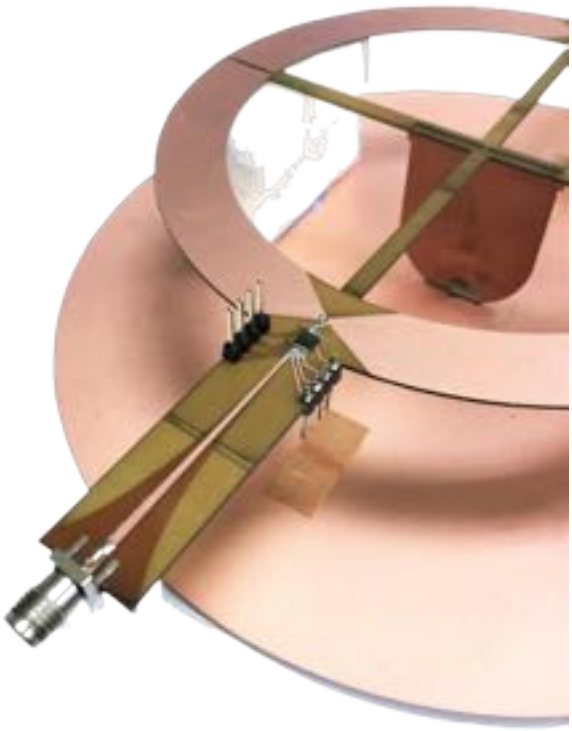

Figure 54 Photo of the fabricated prototype showing the balun's active tuning.

Table IV Comparison of High Isolation PCB STAR Antennas

Work	Frequency	Measured Isolation
[93]	1.6-3.28 GHz	35 dB
[50]	0.8-2.7 GHz	37 dB
[38]	0.5-3.5 GHz	37 dB
[94]	3.5 GHz (55 MHz BW)	40 dB
[54]	3.77 GHz (47 MHz BW)	30 dB
This [95]	1.68-1.93 GHz	31 dB
This (tuned) [95]	**1.68-1.93 GHz**	**42 dB**

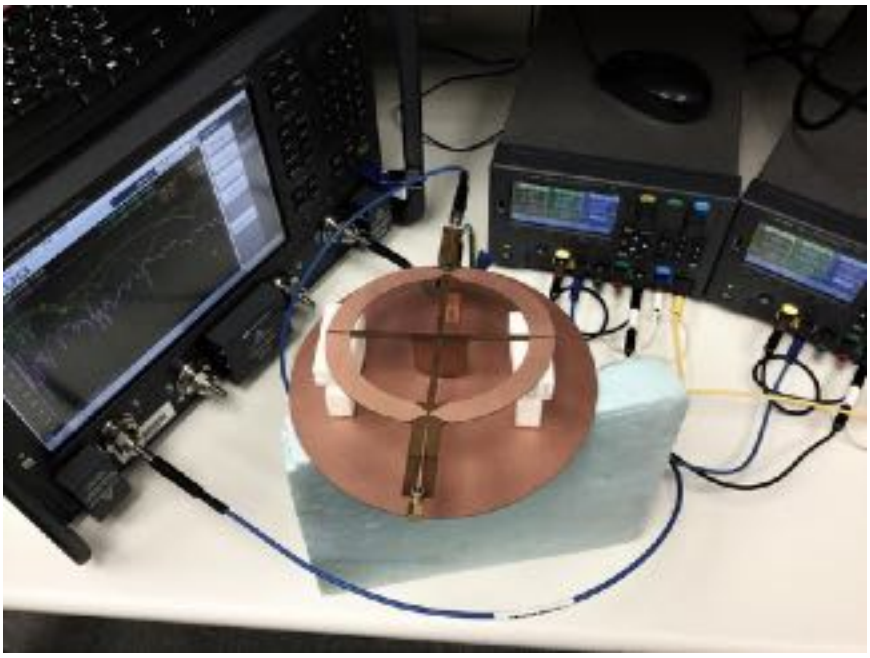

Figure 55 Active STAR balun measurement test bench. The measured VSWR in the active case differed little from the passive case.

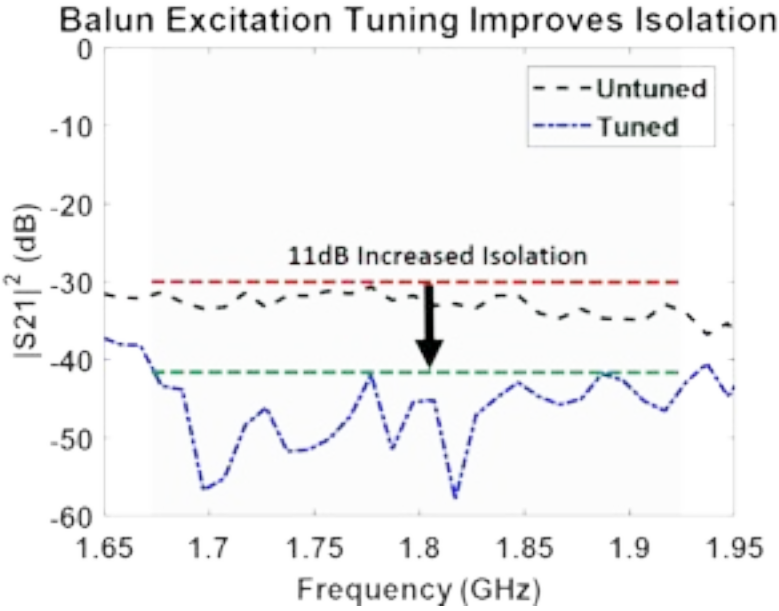

Figure 56 Measured isolation improved by 11 dB across a 250 MHz bandwidth. This performance is the best reported to date.

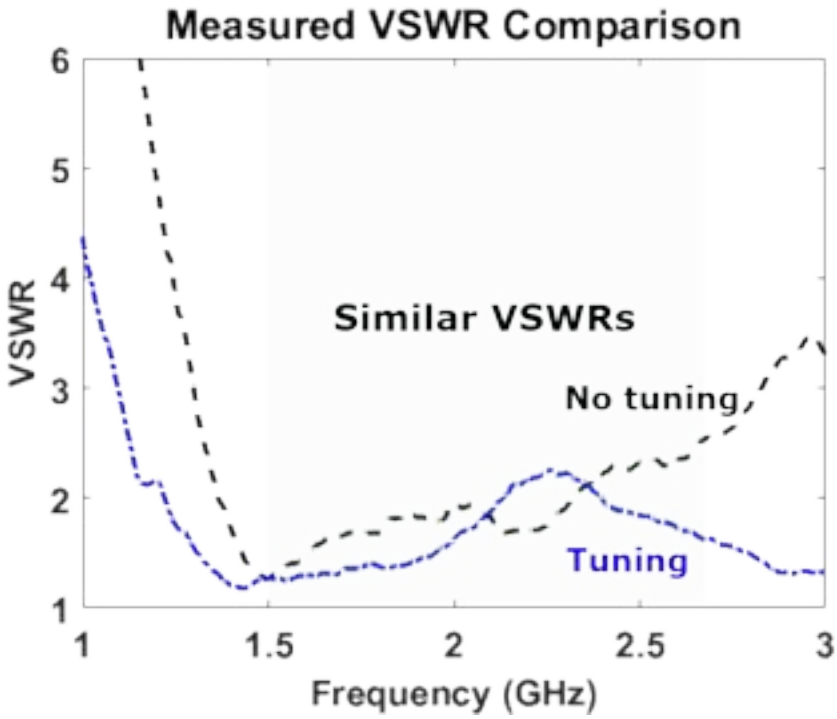

Figure 57 Passive measured and simulated VSWR for the Tx and Rx antennas.

We introduced a novel antenna feed with controllable inserts. The inserts create a current density balance even for geometries with imperfect symmetry. Doing so, we achieved much higher Tx/Rx antenna isolation for Simultaneous Transmit and Receive (STAR) applications. Specifically, even for an antenna with poor isolation, we achieved an additional 11 dB. More importantly, the proposed balanced feed can be used in any antenna to improve its isolation properties and pattern symmetry. This development in STAR is a milestone in novel antenna isolation techniques. It eliminates failures due to unpredictable transmit/receive variations in the antenna.

CHAPTER 5: CONCLUSION

5.1 Summary and Achievements

STAR is a difficult problem due to the precision required to achieve high isolation. To ensure high isolation, both the structural form and electrical excitation signals must be symmetric. Otherwise, the conditions for high isolation are not met.

There is limited availability in the radio frequency (RF) spectrum's 1-6 GHz band. Operating across this bandwidth is advantageous due to its favorable propagation factors and the optimal size for wireless systems, especially mobile devices. Critically, the spectrum is fixed and new frequencies cannot be added.

To operate a wireless network, users must obtain licenses from the FCC. Due to incredibly high demand, licensing fees across the United States are astronomical. In 2015, spectrum was auctioned at a price of $700 per 1 Hz of bandwidth. Practically, this means a single 10 MHz (10,000,000 Hz) channel for 4G LTE corresponds to a $7 billion price tag.

Full-duplex radios are desirable for uplink and downlink. However, concurrent transmission and reception on the same frequency leads to self-interference. Due to path losses from $1/R^2$ power spreading, radio signals are received at extremely low powers, on the order of a billionth or trillionth of the original transmit power. All collocated transceivers experience Tx/Rx leakage, typically on the order of 10 to 30 dB. As such, the power disparity can be 60 dB, or a factor of a million, or greater. This high power leakage obliterates the received signal, making the information undecodable by the receiver. Therefore, this SI must be cancelled.

Several applications could benefit from STAR's double data rates or reduced spectrum footprint, such as point-to-point (P2P) microwave and SCADA links. Cognitive radios and software defined radios can reduce congestion by receive sensing on transmit frequencies.

As radios become agile, changing frequency becomes as simple as a few lines of code. To lower cost, these radios can quickly adapt to data capacity fluctuations. Further, as users grow spectrum congestion becomes acute. These collisions can be eliminated by receive sense on transmit instead of simply detecting that a collision occurred.

Traditional radios were designed from the start for a specific carrier frequency and bandwidth among other considerations. All the chips, antennas, and systems were optimized for those fixed values. However, this process is enormously costly, especially if foundries are involved. If spectrum assignments change, then this process must restart, increasing time and cost.

Twenty first century antenna design unveiled the ultra wideband phased array. Beneficially, they enable beam steering without moving parts and can be fabricated in flat panel form for aesthetic or aerodynamic reasons, making them truly invaluable. Additionally, operation across multiple bands can now be combined into a single antenna.

This class of antennas may be paired with software defined radios (SDRs) that operate across 85:1 or greater bandwidths (e.g. 70 MHz to 6 GHz). To reduce cost, this opens the possibility of spectrum rental where multiple applications may reserve spectrum only when desired.

However, STAR arrays with beam steering capability only existed across narrow bandwidths, on the order of 125 MHz or less. For STAR antennas to be competitive, they

must achieve wide bandwidths and scanning. This is difficult to accomplish. At broadside, symmetry exists across the radiated fields. However, because high isolation arises from symmetry, scanning off the main axis reduces symmetry and therefore isolation. As bandwidth increases, the range of this asymmetry increases.

This work introduced the first wideband phased array antenna for STAR. The 5×5 array of spirals achieved a 35 dB minimum isolation across 1.6-3.28 GHz (2:1 bandwidth). Notably, when scanned to 30°, the isolation dropped by only 3 dB. To achieve a realistic array element, the spirals were miniaturized to half-wavelength diameters by a resistive termination.

Additionally, even greater isolation can be achieved with our novel active feed tuning. This tunable feed improved measured isolation by 11 dB, for a total of 42 dB across 250 MHz (1.68-1.93 GHz). A single chip inserted in each arm of the ring antenna's balun balanced the currents on each arm, increasing electrical symmetry and cancellation. The ability to arbitrarily tune the coupling enabled post-manufacturing correction of fabrication, assembly, and environmental variations that reduced isolation in passive systems.

5.2 Future Work

There are several important research directions in which to proceed: 1) design an amplitude plus phase tunable balun, 2) incorporate tunable baluns into STAR arrays, 3) design automatic tuning control, and 4) achieve cancelation of far environmental reflections with digital filtering.

First, to enable frequency agility regardless of balun characteristics, tuning should include both amplitude and phase. The amplitude may be controlled through fixed or adjustable resistors or attenuator chips. Phase control may be implemented passively through lumped components or tuning stubs or actively via varactors. However, varactors should most likely be placed on the receive chain due to their limited power capability. Additionally, not only would amplitude and phase tuning aid in each element's self-interference cancellation, but could also reduce the Tx interference from adjacent elements. The balun in this work contained a single stage tuning network and achieved a remarkable 250 MHz bandwidth. Further, increasing the number of stages enables greater freedom to tune the input impedance to a wider bandwidth with greater precision.

Second, the balun for a single element can be extended to an array. Due to the miniature size of components, adding tunability does not significantly change the balun's dimensions.

Third, STAR systems will likely contain tuning algorithms to automatically determine the optimal parameters for baluns or RF-SIC filters. One such implementation could involve a training phase to optimize the aforementioned tunable balun. An RF power meter could measure the Tx/Rx coupling across various settings and apply an optimization algorithm.

Fourth, outside of the direct transmit self-interference (SI), the next significant source of SI is from environmental reflections. Due to the desired receive signal's low power, even relatively small objects pose a risk to symmetry. In some cases, the reflected power, even though undergoing $1/R^4$ spreading losses, can have sufficient power to

disrupt the receiver. Several factors make this SI a challenging topic, such as environmental variability and the large delay from distant reflectors.

The following plots demonstrate the effect of environmental reflections on transmit/receive isolation. To reduce perturbations from environmental electrical noise, all of the following measurements were conducted inside an anechoic chamber. A baseline measurement with no reflector achieved an impressive 50 dB isolation across a 100 MHz bandwidth at 2.8 GHz.

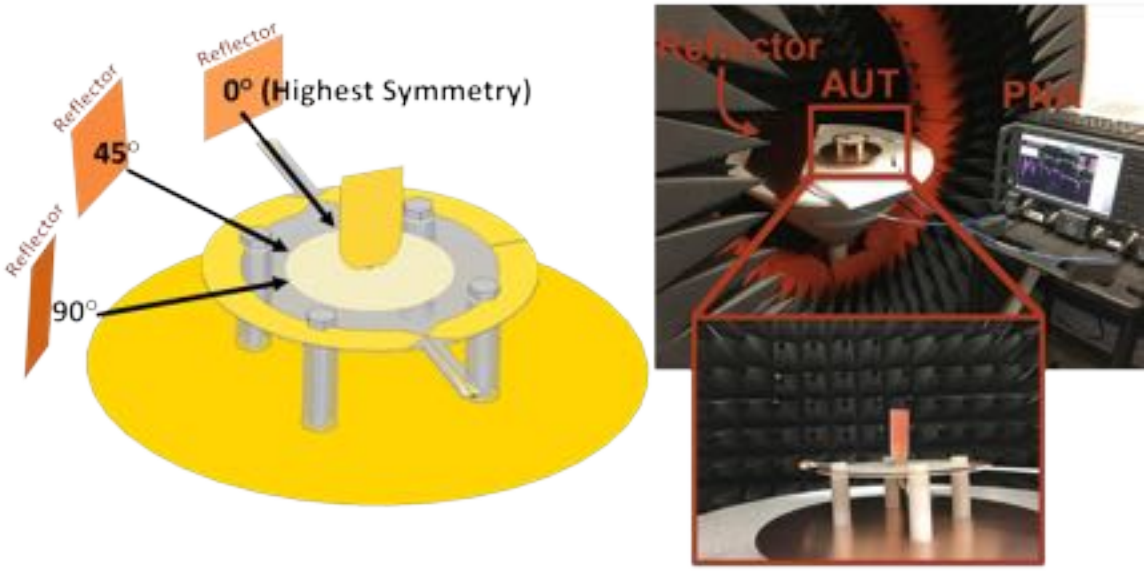

Figure 58 Graphic of the reflector locations at cardinal angles (left) and annotated photos of the antenna in the anechoic chamber. The antenna can be seen on the white foam cone.

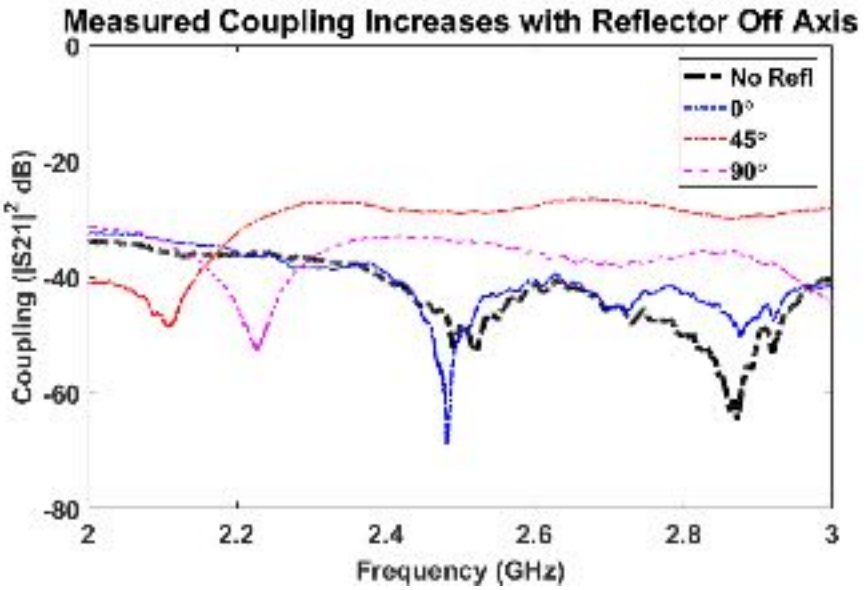

Figure 59 Comparison of Tx/Rx coupling with reflectors at various cardinal angles. All measurements were conducted in an anechoic chamber.

BILIOGRAPHY

[1] https://www.ericsson.com/en/mobility-report/reports/june-2020/mobile-traffic-q1

[2] https://www.ericsson.com/en/mobility-report/reports/june-2020/iot-connections-outlook

[3] https://www.congress.gov/bill/115th-congress/senate-bill/19

[4] https://www.federalregister.gov/documents/2020/10/09/2020-22528/facilitating-shared-use-in-the-3100-3550-mhz-band

[5] FCC "Auction 97 Advanced Wireless Services (AWS-3)," 2015 [Online] wireless.fcc.gov/auctions/default.htm?job=auction_factsheet&id=97.

[6] NTIA "United States Frequency Allocation Chart." https://www.ntia.doc.gov/page/2011/united-states-frequency-allocation-chart.

[7] D. Bharadia, E. McMilin, S. Katti, "Full Duplex Radios," in Proceedings of the ACM SIGCOMM 2013 conference on SIGCOMM, Hong Kong, China, 2013, p.375

[8] S. Bojja Venkatakrishnan, E. A. Alwan and J. L. Volakis, "Wideband RF Self-Interference Cancellation Circuit for Phased Array Simultaneous Transmit and Receive Systems," in IEEE Access, vol. 6, pp. 3425-3432, 2018.

[9] https://aapt.scitation.org/doi/10.1119/1.2238886

[10] IEEE Std 145

[11] S. B. Venkatakrishnan, A. Hovsepian, A. D. Johnson, T. Nakatani, E. A. Alwan and J. L. Volakis, "Techniques for Achieving High Isolation in RF Domain for Simultaneous Transmit and Receive," in IEEE Open Journal of Antennas and Propagation, vol. 1, pp. 358-367, 2020.

[12] MIMOtech, 'Microwave Carrier Ethernet', 2017. [Online]. Available: mimotechnology.com/p_microwave_carrier_ethernet.htm. [Accessed: 17-Jan-2020].

[13] TrellisWare datasheet

[14] J. Zhou and H. Krishnaswamy, "System-level analysis of phase noise in full-duplex wireless transceivers," IEEE Trans. Circuits Syst. II, Exp. Briefs, vol. 65, no. 9, pp. 1189–1193, Sep. 2018.

[15] M. Duarte and A. Sabharwal, "Full-duplex wireless communica- tions using off-the-shelf radios: Feasibility and first results," in Proc. Conf. Rec. 44th Asilomar Conf. Signals Syst. Comput., Nov. 2010, pp. 1558–1562.

[16] D. J. van den Broek, E. A. M. Klumperink, and B. Nauta, “A self- interference-cancelling receiver for in-band full-duplex wireless with low distortion under cancellation of strong TX leakage,” in Proc. IEEE Int. Solid-State Circuits Conf. (ISSCC) Dig. Techn. Papers, Feb. 2015, pp. 1–3.

[17] S. Chen, M. A. Beach, and J. P. McGeehan, “Division-free duplex for wireless applications,” Electron. Lett, vol. 34, no. 2, pp. 147–148, Jan 1998.

[18] M. Jain et al., “Practical, real-time, full duplex wireless,” in Proc. 17th Annu. Int. Conf. Mobile Comput. Netw., 2011, pp. 301–312.

[19] E. Everett, A. Sahai, and A. Sabharwal, “Passive self-interference suppression for full-duplex infrastructure nodes,” IEEE Trans. Wireless Commun., vol. 13, no. 2, pp. 680–694, Feb. 2014.

[20] B. Debaillie et al., “Analog/RF solutions enabling compact full-duplex radios,” IEEE J. Sel. Areas Commun., vol. 32, no. 9, pp. 1662–1673, Sep. 2014.

[21] N. Reiskarimian et al., “One-way ramp to a two-way highway: Integrated magnetic-free nonreciprocal antenna interfaces for full- duplex wireless,” IEEE Microw. Mag., vol. 20, no. 2, pp. 56–75, Feb. 2019.

[22] M. Biedka, Y. E. Wang, Q. M. Xu, and Y. Li, “Full-duplex RF front ends: From antennas and circulators to leakage cancelation,” IEEE Microw. Mag., vol. 20, no. 2, pp. 44–55, Apr. 2020.

[23] I. Brodsky, J. Brand, and M. Jain, “Freedom of frequency: How the quest for in-band full-duplex led to a breakthrough in fil- ter design,” IEEE Microw. Mag., vol. 20, no. 2, pp. 36–43, Feb. 2019.

[24] M. Katanbaf, K. Chu, T. Zhang, C. Su, and J. C. Rudell, “Two-way traffic ahead: RF/analog self-interference cancelation techniques and the challenges for future integrated full-duplex transceivers,” IEEE Microw. Mag., vol. 20, no. 2, pp. 22–35, Feb. 2019.

[25] S. Bojja-Venkatakrishnan, E. A. Alwan, and J. L. Volakis, “Simultaneous transmit and receive system with 1 GHz RF cancellation bandwidth,” in Proc. IEEE Int. Symp. Antennas Propag. USNC/URSI Nat. Radio Sci. Meeting, 2018, pp. 1241–1242.

[26] S. Bojja-Venkatakrishnan, E. A. Alwan, and J. L. Volakis, “Wideband RF and analog self-interference cancelation filter for simultaneous transmit and receive system,” in Proc. IEEE Int. Symp. Antennas Propag. USNC/URSI Nat. Radio Sci. Meeting, Jul. 2017, pp. 933–934.

[27] M. B. Dastjerdi, S. Jain, N. Reiskarimian, A. Natarajan, and

H. Krishnaswamy, “Analysis and design of a full-duplex two-element MIMO circulator-receiver with high TX power handling exploiting MIMO RF and shared-delay baseband self-interference cancellation,” IEEE J. Solid-State Circuits, vol. 54, no. 12, pp. 3525–3540, Dec. 2019.

[28] A. Nagulu and H. Krishnaswamy, “Non-magnetic CMOS switched- transmission-line circulators with high power handling and antenna balancing: Theory and implementation,” IEEE J. Solid-State Circuits, vol. 54, no. 5, pp. 1288–1303, May 2019.

[29] A. Kord, M. Tymchenko, D. L. Sounas, H. Krishnaswamy, and A. Alù, “CMOS integrated magnetless circulators based on spatiotemporal modulation angular-momentum biasing,” IEEE Trans. Microw. Theory Techn., vol. 67, no. 7, pp. 2649–2662, Feb. 2019.

[30] N. Reiskarimian, M. B. Dastjerdi, J. Zhou, and H. Krishnaswamy, “Analysis and design of commutation-based circulator-receivers for integrated full-duplex wireless,” IEEE J. Solid-State Circuits, vol. 53, no. 8, pp. 2190–2201, Aug. 2018.

[31] H. Holma, S. Heikkinen, O. A. Lehtinen, and A. Toskala, “Interference considerations for the time division duplex mode of the UMTS ter- restrial radio access,” IEEE J. Sel. Areas Commun., vol. 18, no. 8, pp. 1386–1393, Aug. 2000.

[32] H. Haas and G. J. R. Povey, “The effect of adjacent channel interference on capacity in a hybrid TDMA/CDMA-TDD system using UTRA-TDD parameters,” in Proc. IEEE VTS 50th Veh. Technol. Conf. (VTC-Fall), vol. 2, 1999, pp. 1086–1090.

[33] K. E. Kolodziej, B. T. Perry, and J. S. Herd, “In-band full-duplex technology: Techniques and systems survey,” IEEE Trans. Microw. Theory Techn., vol. 67, no. 7, pp. 3025–3041, Jul. 2019.

[34] J. Zhou, T. H. Chuang, T. Dinc, and H. Krishnaswamy, “Integrated wideband self-interference cancelation in the RF domain for FDD and full-duplex wireless,” IEEE J. Solid-State Circuits, vol. 50, no. 12, pp. 3015–3031, Dec. 2015.

[35] Z. Zhang, K. Long, A. V. Vasilakos, and L. Hanzo, “Full-duplex wireless communications: Challenges, solutions, and future research directions,” Proc. IEEE, vol. 104, no. 7, pp. 1369–1409, 2016.

[36] J. P. Doane, K. E. Kolodziej, and B. T. Perry, “Simultaneous transmit and receive with digital phased arrays,” in Proc. IEEE Int. Symp. Phased Array Syst. Technol. (PAST), Oct. 2016, pp. 1–6.

[37] A. T. Wegener, "Broadband near-field filters for Simultaneous Transmit and Receive in a small two-dimensional array," 2014 IEEE MTT-S International Microwave Symposium (IMS2014), Tampa, FL, 2014, pp. 1-3.

[38] E. A. Etellisi, M. A. Elmansouri, and D. S. Filipovic, “Wideband monostatic simultaneous transmit and receive (STAR) antenna,” IEEE Trans. Antennas Propag., vol. 64, no. 1, pp. 6–15, Jan. 2016.

[39] J. L. Volakis, M. W. Nurnberger, and D. S. Filipovic, “Slot spiral antenna,” IEEE Antennas Propag. Mag., vol. 43, no. 6, pp. 15–26, Dec. 2001.

[40] B. A. Kramer, M. Lee, C.-C. Chen, and J. L. Volakis, “Design and performance of an ultrawide-band ceramic-loaded slot spiral,” IEEE Trans. Antennas Propag., vol. 53, no. 7, pp. 2193–2199, Jul. 2005.

[41] M. Akbari, H. A. Ghalyon, M. Farahani, A. Sebak, and T. A. Denidni, “Spatially decoupling of CP antennas based on FSS for 30-GHz MIMO systems,” IEEE Access, vol. 5, pp. 6527–6537, 2017.

[42] X. Yang, Y. Liu, Y. Xu, and S. Gong, “Isolation enhancement in patch antenna array with fractal UC-EBG structure and cross slot,” IEEE Antennas Wireless Propag. Lett., vol. 16, pp. 2175–2178, 2017.

[43] T. Dabas, D. Gangwar, B. K. Kanaujia, and A. Gautam, “Mutual coupling reduction between elements of UWB MIMO antenna using small size uniplanar EBG exhibit- ing multiple stop bands,” AEU Int. J. Electron. Commun., vol. 93, pp. 32–38, Sep. 2018. [Online]. Available: http://www.sciencedirect.com/science/article/pii/S1434841117328352

[44] P. V. Prasannakumar, M. A. Elmansouri, and D. S. Filipovic, “Wideband decoupling techniques for dual-polarized bi-static simulta- neous transmit and receive antenna subsystem,” IEEE Trans. Antennas Propag., vol. 65, no. 10, pp. 4991–5001, Oct. 2017.

[45] G. Zhai, Z. N. Chen, and X. Qing, “Mutual coupling reduction of a closely spaced four-element MIMO antenna system using discrete mushrooms,” IEEE Trans. Microw. Theory Tech., vol. 64, no. 10, pp. 3060–3067, Oct. 2016.

[46] G. Zhai, Z. N. Chen, and X. Qing, “Enhanced isolation of a closely spaced four-element MIMO antenna system using metamaterial mush- room,” IEEE Trans. Antennas Propag., vol. 63, no. 8, pp. 3362–3370, Aug. 2015.

[47] K. E. Kolodziej, P. T. Hurst, A. J. Fenn and L. I. Parad, "Ring array antenna with optimized beamformer for Simultaneous Transmit And Receive," Proceedings of the 2012 IEEE International Symposium on Antennas and Propagation, Chicago, IL, 2012, pp. 1-2.

[48] M. A. Elmansouri; A. J. Kee; D. S. Filipovic, "Wideband Antenna Array for Simultaneous Transmit and Receive (STAR) Applications," IEEE Antennas and Wireless Propagation Letters, 2017.

[49] E. A. Etellisi, M. A. Elmansouri and D. S. Filipović, "Wideband simultaneous transmit and receive (STAR) circular array system," 2016 IEEE International Symposium on Phased Array Systems and Technology (PAST), Waltham, MA, 2016, pp. 1-5.

[50] E. Yetisir, C. C. Chen and J. L. Volakis, "Wideband Low Profile Multiport Antenna With Omnidirectional Pattern and High Isolation," in IEEE Transactions on Antennas and Propagation, vol. 64, no. 9, pp. 3777-3786, Sept. 2016.

[51] J. P. Doane, K. E. Kolodziej and B. T. Perry, "Simultaneous transmit and receive performance of an 8-channel digital phased array," 2017 IEEE International Symposium on Antennas and Propagation & USNC/URSI National Radio Science Meeting, San Diego, CA, 2017, pp. 1043-1044.

[52] J. Huang, "Dual-Polarised Microstrip Array with High isolation and Low Cross-Polarisation," Microwave and Optical Technology Letters., Vol. & February 1991, pp 99-102

[53] M. J. Cryan and P. S. Hall, "Integrated active antenna with simultaneous transmit-receive operation," in Electronics Letters, vol. 32, no. 4, pp. 286-287, 15 Feb. 1996, doi: 10.1049/el:19960225.

[54] M. J. Cryan and P. S. Hall, "Integrated active antenna with simultaneous transmit-receive operation," IEEE Antennas and Propagation Society International Symposium. 1996 Digest, Baltimore, MD, USA, 1996, pp. 1314-1317 vol.2, doi: 10.1109/APS.1996.549838.

[55] M. J. Cryan, P. S. Hall, K. S. H. Tsang and J. Sha, "Integrated active antennas with simultaneous transmit-receive operation," 1996 26th European Microwave Conference, Prague, Czech Republic, 1996, pp. 565-568, doi: 10.1109/EUMA.1996.337644.

[56] S. L. Karode and V. F. Fusco, "Dual polarised microstrip patch antenna using feedforward isolation enhancement for simultaneous transmit/receive applications," IEE National Conference on Antennas and Propagation, York, UK, 1999, pp. 49-52, doi: 10.1049/cp:19990013.

[57] A. Raghavan, E. Gebara, M. Tentzeris and J. Laskar, "An active interference canceller for multistandard collocated radio," IEEE MTT-S International Microwave Symposium Digest, 2005., Long Beach, CA, 2005, pp. 4 pp.-726, doi: 10.1109/MWSYM.2005.1516712.

[58] S. Cheung, T. Halloran, W. Weedon and C. Caldwell, "Active quasi-circulators using quadrature hybrids for simultaneous transmit and receive," 2009 IEEE MTT-S International Microwave Symposium Digest, Boston, MA, 2009, pp. 381-384.

[59] S. K. Cheung, T. P. Halloran, W. H. Weedon and C. P. Caldwell, "MMIC-Based Quadrature Hybrid Quasi-Circulators for Simultaneous Transmit and Receive," in IEEE Transactions on Microwave Theory and Techniques, vol. 58, no. 3, pp. 489-497, March 2010.

[60] S. K. Cheung, W. H. Weedon and C. P. Caldwell, "High isolation lange-ferrite circulators with NF suppression for simultaneous transmit and receive," 2010 IEEE MTT-S International Microwave Symposium, Anaheim, CA, 2010, pp. 1352-1355.

[61] C. H. Cox and E. I. Ackerman, "Photonics for simultaneous transmit and receive," 2011 IEEE MTT-S International Microwave Symposium, Baltimore, MD, 2011, pp. 1-4.

[62] C. Cox and E. Ackerman, "Demonstration of a single-aperture, full-duplex communication system," 2013 IEEE Radio and Wireless Symposium, Austin, TX, 2013, pp. 148-150.

[63] C. H. Cox and E. I. Ackerman, "TIPRx: A Transmit-Isolating Photonic Receiver," in Journal of Lightwave Technology, vol. 32, no. 20, pp. 3630-3636, 15 Oct.15, 2014.

[64] A. T. Wegener and W. J. Chappell, "Simultaneous Transmit And Receive with a small planar array," 2012 IEEE/MTT-S International Microwave Symposium Digest, Montreal, QC, 2012, pp. 1-3.

[65] A. T. Wegener and W. J. Chappell, "Coupled antenna scheme using filter design techniques and tunable resonators to show simultaneous transmit and receive," 2013 IEEE MTT-S International Microwave Symposium Digest (MTT), Seattle, WA, 2013, pp. 1-4.

[66] A. T. Wegener and W. J. Chappell, "High isolation in antenna arrays for simultaneous transmit and receive," 2013 IEEE International Symposium on Phased Array Systems and Technology, Waltham, MA, 2013, pp. 593-597.

[67] J. I. Choi, M. Jain, K. Srinivasan, P. Levis, and S. Katti, “Achieving single channel, full duplex wireless communication,” International Conference on Mobile Computing and Networking, vol. 16, no. 6,pp. 1â€“12, September 2010.

[68] T. Snow, C. Fulton and W. J. Chappell, "Transmit & Receive Duplexing Using Digital Beamforming System to Cancel Self-Interference," in IEEE Transactions on Microwave Theory and Techniques, vol. 59, no. 12, pp. 3494-3503, Dec. 2011, doi: 10.1109/TMTT.2011.2172625.

[69] S. E. Johnston and P. D. Fiore, "Full-duplex communication via adaptive nulling," 2013 Asilomar Conference on Signals, Systems and Computers, Pacific Grove, CA, 2013, pp. 1628-1631.

[70] K. E. Kolodziej, J. G. McMichael and B. T. Perry, "Adaptive RF canceller for transmit-receive isolation improvement," 2014 IEEE Radio and Wireless Symposium (RWS), Newport Beach, CA, 2014, pp. 172-174, doi: 10.1109/RWS.2014.6830069.

[71] S. Enserink et al., "Joint Analog and Digital Interference Cancellation," 2014 IEEE International Symposium on Dynamic Spectrum Access Networks (DYSPAN), McLean, VA, 2014, pp. 378-379.

[72] L. Li, K. Josiam and R. Taori, "Feasibility study on full-duplex wireless millimeter-wave systems," 2014 IEEE International Conference on Acoustics, Speech and Signal Processing (ICASSP), Florence, 2014, pp. 2769-2773.

[73] K. E. Kolodziej, J. G. McMichael and B. T. Perry, "Simultaneous transmit and receive antenna isolation improvement in scattering environments," 2014 IEEE Antennas and Propagation Society International Symposium (APSURSI), Memphis, TN, 2014, pp. 2228-2229.

[74] A. J. Stark, K. Davis, C. Ward and J. Gray, "Photonics for electronic warfare," 2014 IEEE Avionics, Fiber-Optics and Photonics Technology Conference (AVFOP), Atlanta, GA, 2014, pp. 3-4.

[75] T. Dinc and H. Krishnaswamy, "A T/R antenna pair with polarization-based reconfigurable wideband self-interference cancellation for simultaneous transmit and receive," 2015 IEEE MTT-S International Microwave Symposium, Phoenix, AZ, 2015, pp. 1-4.

[76] E. A. Etellisi, M. A. Elmansouri and D. S. Filipovic, "Wideband simultaneous transmit and receive (STAR) bi-layer circular array," 2015 IEEE International Symposium on Antennas and Propagation & USNC/URSI National Radio Science Meeting, Vancouver, BC, 2015, pp. 2227-2228.

[77] M. A. Elmansouri, E. A. Etellisi and D. S. Filipovic, "Ultra-wideband circularly-polarized simultaneous transmit and receive (STAR) antenna system," 2015 IEEE International Symposium on Antennas and Propagation & USNC/URSI National Radio Science Meeting, Vancouver, BC, 2015, pp. 508-509.

[78] A. Sabharwal, P. Schniter, D. Guo, D. W. Bliss, S. Rangarajan and R. Wichman, "In-Band Full-Duplex Wireless: Challenges and Opportunities," in IEEE Journal on Selected Areas in Communications, vol. 32, no. 9, pp. 1637-1652, Sept. 2014.

[79] K. E. Kolodziej, B. T. Perry and J. S. Herd, "Simultaneous Transmit and Receive (STAR) system architecture using multiple analog cancellation layers," 2015 IEEE MTT-S International Microwave Symposium, Phoenix, AZ, 2015, pp. 1-4.

[80] P. V. Prasannakumar, M. A. Elmansouri and D. S. Filipovic, "High-Directivity Broad Band Simultaneous Transmit and Receive (STAR) Antenna System," 2018 IEEE International Symposium on Antennas and Propagation & USNC/URSI National Radio Science Meeting, Boston, MA, 2018, pp. 387-388.

[81] M. E. Knox, "Single antenna full duplex communications using a common carrier," WAMICON 2012 IEEE Wireless & Microwave Technology Conference, Cocoa Beach, FL, 2012, pp. 1-6.

[82] S. Perlman, L. Kelley, W. Russell and W. Stuart, "Concerning Optimum Frequencies for Space Vehicle Communication," in IRE Transactions on Communications Systems, vol. 7, no. 3, pp. 167-173, September 1959.

[83] J. Huang "Dual-Polarised Microstrip Array with High Isolation and Low Cross Polarization" Microwave and Optical Technology Letters vol. 4 no. 3 pp. 99-103 October 1991.

[84] A. Hovsepian, S. B. Venkatakrishnan, E. A. Alwan and J. L. Volakis, "Wideband, scanning array for simultaneous transmit and receive," 2018 International Applied Computational Electromagnetics Society Symposium (ACES), Denver, CO, 2018, pp. 1-2.

[85] A. Hovsepian, E. A. Alwan and J. L. Volakis, "Wideband scanning array of spiral antennas for simultaneous transmit and receive (STAR)," 2017 IEEE International Symposium on Antennas and Propagation & USNC/URSI National Radio Science Meeting, San Diego, CA, 2017, pp. 487-488.

[86] A. Hovsepian, S. B. Venkatakrishnan, E. A. Alwan and J. L. Volakis, "Wideband Beam Steering Using a 4-Arm Spiral Array for Simultaneous Transmit and Receive (STAR) Operation," 2018 IEEE International Symposium on Antennas and Propagation & USNC/URSI National Radio Science Meeting, Boston, MA, 2018, pp. 1915-1916.

[87] M. W. Nurnberger and J. L. Volakis, "New termination for ultrawide-band slot spirals," in IEEE Transactions on Antennas and Propagation, vol. 50, no. 1, pp. 82-85, Jan 2002.

[88] J. Dyson, "The equiangular spiral antenna," in IRE Transactions on Antennas and Propagation, vol. 7, no. 2, pp. 181-187, April 1959.

[89] ROHACELL, “Negligible Absorption in the High Frequency Range,” 2019. [Online]. Available: www.rohacell.com/product/rohacell/en/products-services/rohacell-hf/ [Accessed: Dec 28, 2019].

[90] E. Yetisir, C. Chen and J. L. Volakis, "Wideband dual-polarized omnidirectional antenna with very high isolation across 1.65–2.7 GHz," 2014 IEEE Antennas and Propagation Society International Symposium (APSURSI), Memphis, TN, 2014, pp. 1123-1124.

[91] N. Marchand, "Transmission Line CONVERSION TRANSFORMERS", Electronics, Vol 17, December 1944, pp. 142-145.

[92] Analog Devices. “HMC346AMS8GE” 2020 [Online]
https://www.analog.com/en/products/hmc346ams8ge.html.

[93] A. Hovsepian, E. A. Alwan and J. L. Volakis, "A Wideband, Scanning Array of Four-Arm Spiral Elements for Simultaneous Transmit and Receive," in IEEE Antennas and Wireless Propagation Letters, vol. 19, no. 4, pp. 537-541, April 2020.

[94] A. T. Wegener, "Broad Band near-field filters for Simultaneous Transmit and Receive in a small two-dimensional array," 2014 IEEE MTT-S International Microwave Symposium (IMS2014), Tampa, FL, 2014, pp. 1-3.

[95] A. Hovsepian, S. B. Venkatakrishnan and J. L. Volakis, "Active Feed Tuning for Excitation Symmetry in Simultaneous Transmit and Receive Antennas," in IEEE Antennas and Wireless Propagation Letters, doi: 10.1109/LAWP.2020.3033489.

VITA

ALEXANDER HOVSEPIAN

2010-2015	B.S., Electrical Engineering University of Washington Seattle, Washington
2015-2017	M.S., Electrical & Computer Engineering The Ohio State University Columbus, Ohio
2017-2020	Ph.D., Electrical & Computer Engineering Florida International University Miami, Florida

PUBLICATIONS AND PRESENTATIONS

Hovsepian, A., Alwan, E. A., Volakis, J. L. (2020). *A Wideband, Scanning Array of Four-Arm Spiral Elements for Simultaneous Transmit and Receive*. IEEE Antennas and Wireless Propagation Letters, 19 (4):537-541.

Hovsepian, A., Venkatakrishnan, S. B., Volakis, J. L. (2020). *Active Feed Tuning for Excitation Symmetry in Simultaneous Transmit and Receive Antennas*. IEEE Antennas and Wireless Propagation Letters, Accepted for Publication.

A. Hovsepian, S. B. Venkatakrishnan, and J. L. Volakis, "Active Excitation Tuning for Simultaneous Transmit and Receive Antennas," IEEE Intl. Symposium on Antennas and Propagation & USNC/URSI National Radio Science Meeting (APS/URSI), Montreal, QC, 2020. (virtual)

A. Hovsepian, S. B. Venkatakrishnan, and J. L. Volakis, "Transmit-Receive Antenna Isolation Using a Passively Tuned Balun for Simultaneous Transmit and Receive (STAR) Applications," IEEE Intl. Symposium on Antennas and Propagation & USNC/URSI National Radio Science Meeting (APS/URSI), Atlanta, GA, 2019.

A. Hovsepian, S. B. Venkatakrishnan, E. A. Alwan, and J. L. Volakis, "Port to Port Isolation of an Omnidirectional Antenna Through Perfect Symmetry for Simultaneous Transmit and Receive (STAR)," USNC-URSI National Radio Science Meeting, Boulder, CO, 2019.

A. Hovsepian, S. B. Venkatakrishnan, E. A. Alwan, and J. L. Volakis, "Wideband, scanning array for simultaneous transmit and receive," International Applied

Computational Electromagnetics Society Symposium (ACES), Denver, CO, 2018. https://ieeexplore.ieee.org/document/8364164

A. Hovsepian, S. B. Venkatakrishnan, E. A. Alwan, and J. L. Volakis, "Wideband Beam Steering Using a 4-Arm Spiral Array for Simultaneous Transmit and Receive (STAR) Operation," IEEE Intl. Symposium on Antennas and Propagation & USNC/URSI National Radio Science Meeting (APS/URSI), Boston, MA, 2018.
https://ieeexplore.ieee.org/document/8608797

A. Hovsepian, S. B. Venkatakrishnan, E. A. Alwan, and J. L. Volakis, "Wideband Scanning STAR Array," USNC-URSI National Radio Science Meeting, Boulder, CO, 2018.

A. Hovsepian, E. A. Alwan, and J. L. Volakis, "Wideband scanning array of spiral antennas for simultaneous transmit and receive (STAR)," IEEE Intl. Symposium on Antennas and Propagation & USNC/URSI National Radio Science Meeting (APS/URSI), San Diego, CA, 2017. https://ieeexplore.ieee.org/abstract/document/8072286

A. Hovsepian, E. A. Alwan, and J. L. Volakis, "Wideband Phased Array of Spiral Antennas for Simultaneous Transmit and Receive (STAR)," USNC-URSI National Radio Science Meeting, Boulder, CO, 2017.

E. A. Alwan, A. Hovsepian, and J. L. Volakis, "Ultra-wideband dual polarization arrays with collocated elements for high isolation simultaneous transmit and receive systems," IEEE Intl. Symposium on Phased Array Systems and Technology (PAST), Waltham, MA, 2016. https://ieeexplore.ieee.org/document/7832608

A. Hovsepian, E. A. Alwan, and J. L. Volakis, "High Isolation Ultra Wideband Dual Polarization Arrays for Simultaneous Transmit and Receive Systems," IEEE Intl. Symposium on Antennas and Propagation & USNC-URSI National Radio Science Meeting (APS/URSI), Fajardo, Puerto Rico, 2016.